Deactivation Kinetics of Solid Acid Catalyst with Laterally Interacting Protons

Aditya Sengar,[†] Rutger A. van Santen,*,[†,‡] Erik Steur,[‡,§] Johannes A. M. Kuipers,[†] and Johan Padding[∥]

[†]Department of Chemical Engineering and Chemistry, Eindhoven University of Technology, P.O. Box 513, 5600 MB Eindhoven, The Netherlands

[‡]Institute for Complex Molecular Systems, Eindhoven University of Technology, P.O. Box 513, 5600 MB Eindhoven, The Netherlands

[§]Delft Center for Systems and Control, Delft University of Technology, Mekelweg 2, 2628 CD Delft, The Netherlands

[∥]Process and Energy Department, Delft University of Technology, Leeghwaterstraat 39, 2628 CB Delft, The Netherlands

ⓢ *Supporting Information*

ABSTRACT: Differences in catalyst deactivation kinetics in solid acid catalysis are studied with catalyst models that allow for lateral interaction between protons. Deactivation of a solid acid catalyst with laterally interacting protons induces inhomogeneity of proton reactivity that develops with time. As a consequence, product selectivity changes and deactivation will accelerate. This is demonstrated by simulations of the deactivation kinetics of the alkylation reaction of propylene with isobutane. The effect of lateral interactions between protons arises because initial catalyst deactivation is not caused by pore blocking or coke deposition but by a molecular

mechanism where protons are consumed due to the formation of stable nonreactive carbenium ions. High selectivity to alkylate requires a catalyst with protons of high reactivity. When protons become consumed by formation of stable deactivating carbenium ions, initially reactive protons are converted into protons of lower reactivity. The latter only catalyze deactivating oligomerization reactions. Simulations that compare the deactivation kinetics of a catalyst model with laterally interacting protons and a catalyst model that contains protons of similar but different reactivity, but that do not laterally interact, are compared. These simulations demonstrate that the lateral interaction catalyst model is initially more selective but also has a lower stability. Catalyst deactivation of the alkylation reaction occurs through two reaction channels. One reaction channel is due to oligomerization of reactant propylene. The other deactivation reaction channel is initiated by deprotonation of intermediate carbenium ions that increase alkene concentration. By consecutive reactions, this also leads to deactivation. The hydride transfer reaction competes with oligomerization reactions. It is favored by strongly acid sites that also suppress the deprotonation reaction. Within the laterally interacting proton catalyst model, when reactive protons become deactivated, weakly reactive protons are generated that only catalyze the deactivating alkene oligomerization and consecutive reactions. This rapid formation of the weakly reactive protons is the cause of decreasing selectivity with reaction time and increased rate of deactivation. Solutions of the mean field kinetic equations as well as stochastic simulations are presented. Comparative simulations with a reduced number of neighbors of the protons illustrate decreased deactivation rates when the proton density decreases. Island formation of adsorbed reaction intermediates on the catalyst surface is observed in stochastic kinetics simulations. When alkylation selectivity is high, this island formation increases the rate of catalyst deactivation in comparison to the rate of deactivation according to the mean field studies. A nonlinear dynamics model of proton dynamics is provided, which shows that the differences between stochastic and mean field simulations are due to frustrated proton state percolation.

KEYWORDS: alkylation catalysis, solid acid catalysis, catalyst deactivation, laterally interacting protons, kinetics simulations, nonlinear dynamics, site percolation
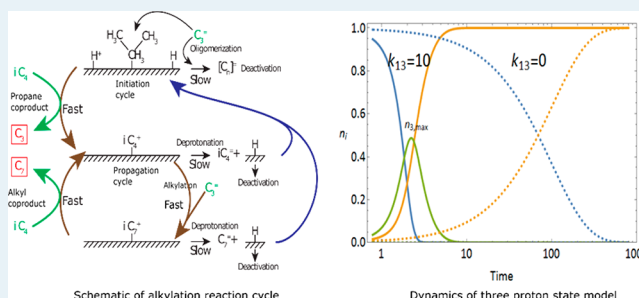
1. INTRODUCTION

Surface chemical reactivity is strongly affected by lateral interactions between chemisorbed reaction intermediates. Then, for a catalytically reactive surface, sites of activity cannot be considered to behave independently. On transition metals, it may lead to collective phenomena such as surface island overlayer formation or dynamic phenomena such as time-dependent oscillatory reaction kinetics.[1]

The physical chemistry of lateral interactions of protons in solid acid catalysis has been much less investigated. However, it has become understood that the close presence of protons near each other tends to enhance their reactivity.

Classical ion exchange experiments demonstrate a reduction in intrinsic proton reactivity when protons become exchanged by cations. It induces a strengthening of the proton bond zeolite framework mainly caused by the negative charge that is generated on the zeolite framework.[2] This was also demonstrated by early quantum-chemical calculations with cluster models of the zeolite framework.[3] A recent experimental study on methanol activation shows enhanced reactivity with high proton concentration.[4] Enhanced catalyst deactivation when the proton concentration is greater is found in a model study of the methanol to olefin (MTO) reaction.[5]

For the alkylation reaction of propylene and isobutane that is catalyzed by solid acid catalysts, we will computationally study catalyst deactivation as a function of proton concentration. Proton reactivity differences can be caused by changes in framework composition or structure of the zeolite. Instead, in the simulations that we present, zeolite framework composition is not altered and proton reactivity differences are due to a proton-removing reaction caused by a nonselective deactivating reaction.

Whereas often pore or site blocking, which may cause mass transfer limitations, are the cause of accelerated deactivation,[6] for the low-temperature alkylation reaction such deactivation is initially not dominant. A molecular mechanism then initiates catalyst deactivation.

Alkylation of propylene or *n*-butene with isobutane is a widely used refinery process, based on neat sulfuric acid or hydrogen fluoride as catalyst. In this low-temperature reaction, branched C_7 or C_8 alkanes (the alkylate) are formed as useful high-octane fuel. Replacement of this homogeneous process by a heterogeneous process is highly desirable.[7] The main drawback of the use of a heterogeneous solid acid catalyst is its short catalyst lifetime of approximately 10 h.[8,9]

Experimental studies of deactivation kinetics of this reaction show, after an initial period of selective alkylate formation, accelerated deactivation and a delayed production of oligomerization product.[10,11] Research on the recently developed Alkyl Clean process[12,13] has demonstrated that the initial deactivation is due to the formation of deactivating hydrocarbons that can be readily removed in a successive low-temperature hydrogenation reaction step.

The delayed production of alkene oligomers and high reactivity of deactivating adsorbed coproduct molecules indicate that the deactivation mechanism has a molecular chemical origin. When pore blocking and mass transfer limitations would cause deactivation, oligomerization would not continue after alkylate production has decayed. We will present model deactivation kinetics simulations that show such an accelerated decline of alkylate production and overshoot of oligomer production.

The low-temperature deactivation of the alkylation reaction is different from the deactivation kinetics of high-temperature solid acid catalytic reactions such as catalytic cracking and the MTO reaction, where deactivation is dominated by pore or site blocking of the zeolite catalyst micropores by deposition of a carbonaceous residue of low reactivity, which has to be oxidatively removed.[14−16] An additional reason for accelerated decay is the often inhomogeneous reactant and product distribution in catalytic plug flow reactors.[17] This is critical to

alkylation deactivation kinetics where alkene concentration has to be kept low. It is this reason that the alkylation reaction is preferentially performed in a slurry reactor or continuously stirred tank reactor (CSTR). Comparison of plug flow reactor data with CSTR data shows an increase in lifetime from 30 min to 15 h.[18]

The fundamental reason that in many solid acid catalyzed reactions catalyst deactivation is rapid is the usual presence of alkenes as rthe eactant, reaction intermediate, or product. Even when saturated molecules are converted as, for example, alkanes in the catalytic cracking reaction or methanol in the MTO reaction, alkenes will be formed as reaction intermediates.[19,20]

Alkenes are highly reactive and will readily oligomerize. They are often desirable reaction intermediates, but apart from leading to formation of desired product, they will, through successive reactions, also produce deactivating carbonaceous residue or coke.[20] In the alkylation reaction, this problem is even more severe since propylene or *n*-butene is used as a reactant.

Different from high-temperature catalysis, where catalyst deactivation is mainly due to coke deposition, catalyst deactivation of the alkylation reaction is initially dominated by proton consumption. It is the result of a competitive chain of reactions of unsaturated reaction intermediate molecules that is related to the paring reaction.[11,21−23] Proton consumption then is due to the formation of stable substituted cyclopentadienyl positively charged carbenium ions. This happens when the Lewis basicity of the deprotonated zeolite framework reaction center is less than the reaction intermediate that becomes protonated. Not only will the proton consumption reduce the surface concentration of the protons that are left but also these protons will also have reduced intrinsic reactivity. This is, among other things, due to the previously mentioned negative charge that proton removal generates on the zeolite lattice.

We will conclude this introductory section with a short summary of the current understanding of the molecular mechanism of the alkylation reaction. It will provide an opportunity to introduce the two reaction channels that are the main cause of catalyst deactivation. We will, at the close of this section, also introduce the laterally interacting proton model that is the core topic of the paper.

Several catalytic reaction cycles combine to convert alkene and isobutane into alkylate. The complex network of the alkylation reaction is reasonably well understood. We will base our model on the catalytic mechanism of the reaction previously presented[13,24] and the earlier founding work by Schmerling.[25]

In a previous paper, we have extensively studied the full reaction mechanism of the alkylation reaction of propylene and isobutane to give C_7 and C_8 isomers using quantum chemically calculated elementary reaction rate constants of the many elementary reaction steps that constitute the corresponding catalytic cycles.[26] These elementary reaction rate constants then have been applied in microkinetic simulations of the complete reaction system. The information deduced from these microkinetic simulations will be used here as input to the lumped kinetics simulations. In order to make the analysis of the deactivation kinetics tractable, the kinetic simulations will be based on a simplified, but useful, version of the alkylation reaction cycle.

A schematic representation of this cycle is shown in Figure 1, which is useful to discuss the kinetic conditions that determine high alkylate selectivity and slow catalyst deactivation.

The reaction consists of an initiation cycle and a propagation cycle. As we will see, no deactivation will occur when the
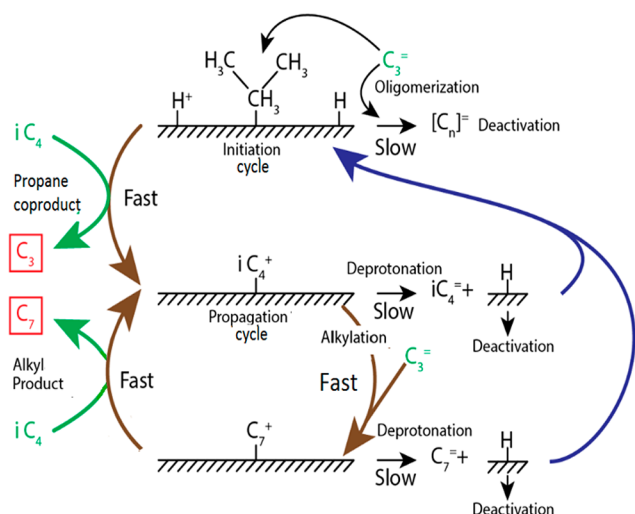
Figure 1. Scheme of the alkylation reaction cycle including deactivation reaction paths. Desirable rate relations are indicated for high selectivity of alkylate and slow deactivation rate.

propagation cycle has no feed-forward loop connection with the reaction initiation cycle.

The alkylation reaction starts with adsorption of propylene to a proton. This results in a propyl carbenium cation that becomes adsorbed to the surface as an alkoxy intermediate. The propyl carbenium ion initiates the alkylation reaction by consecutive reaction with isobutane that gives (undesirable) propane as a product and the desirable isobutyl cation as reaction intermediate. It will depend on the specific zeolite whether this carbenium ion will remain adsorbed to the surface or will be a carbenium ion intermediate that nearly freely rotates and weakly interacts with the surface.[27,28]

In the initiation reaction, the reaction of the propyl cation with another propylene molecule that gives a protonated oligomer competes with the formation of the isobutyl cation by reaction of isobutane. The oligomerization reaction will initiate consecutive reactions that deactivate the catalyst.

The reaction of isobutane with the propyl cation is an example of a hydride transfer reaction. Transfer of the hydride ion

converts the propyl cation into propane. The isobutyl cation intermediate that is cogenerated from isobutane now carries a positive charge. As long as the rates of the respective hydride transfer reactions are fast, deactivation will be suppressed and alkylate selectivity will be high.

The hydride transfer reaction has been quantum chemically well investigated.[26,29,30] Especially when larger carbenium ions are involved, the corresponding reaction intermediates can be considered as nearly freely moving. Their formation has relatively low activation barriers when proton reactivity is large.[19] Transition states of the alkene oligomerization reaction have more constrained mobility and a stronger interaction with the proton reaction center and are hence less proton reactivity demanding.[19,31] Therefore, competition between hydride transfer and oligomerization reactions is in favor of the hydride transfer reaction when it is catalyzed by highly reactive proton sites.[10,26]

Once isobutyl cations are formed, the propagation reaction cycle begins. The isobutyl cation reacts with a propylene molecule to give a C_7^+ cation. In the next reaction step, hydride transfer with isobutane will produce the C_7 alkylate molecule and the isobutyl cation will be regenerated. The propagation cycle continues by a following reaction of the isobutyl cation with another propylene molecule etc.

The isobutyl cation can be considered the organo-catalyst of the propagation reaction cycle. In this propagation reaction cycle, the proton does not play an explicit role.

The role of the proton becomes different when parasitic deprotonation reactions occur that convert the iC_4^+ cation and C_7^+ cation to their respective olefins. Then a proton is back-donated to the solid. The rate of deprotonation reactions becomes suppressed by competitive hydride transfer reactions of the C_7^+ or iC_4^+ cations with isobutane.

The occurrence of the deprotonation reactions opens a second deactivation channel next to that propylene oligomerization. The olefins produced by deprotonation will also initiate consecutive oligomerization reaction that deactivate the catalyst.

Additionally, a feed-forward loop with the reaction initiation cycle opens due to regeneration of protons. This will reinitiate the initiation reaction channel that competes with the deactivating propylene oligomerization.
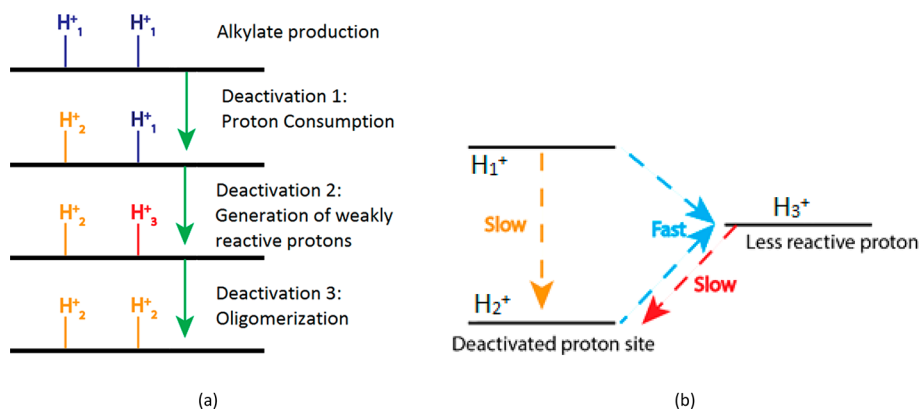
Figure 2. Schematic illustration of the laterally interacting two proton reactivity catalyst model: the dual interacting proton catalyst model. (a) Illustration of the three proton states: reactive state H_1^+ that catalyzes alkylate production, deactivated state H_2^+ with no reactivity, and the state H_3^+, where the proton has lower reactivity and will only catalyze alkene oligomerization. (b) Dynamics of proton deactivation in the dual interacting proton catalyst model. Deactivation of the reactive H_1^+ proton state by catalytic reactions is slow, but once a deactivated proton state H_2^+ is a neighbor, a proton in its H_1^+ state is rapidly converted into a proton in the less reactive H_3^+ state. The latter also deactivates slowly by catalysis but only catalyzes oligomerization and consecutive deactivating reactions.

Theoretically, the alkylation catalyst will be infinitely stable as long as deprotonation of intermediate carbenium ions does not occur, since then the initiation reaction cycle will not be reactivated.

In the following sections, detailed kinetic simulations will be presented on the basis of the mechanistic principles discussed here and illustrated in Figure 1. Catalyst models will be compared with laterally interacting and noninteracting protons. For further comparison we will also present kinetics simulations as a function of proton concentration.

The laterally interacting proton catalyst model that we will use is illustrated in Figures 2. This dual interacting proton catalyst model simplifies differences in reactivity between protons to only two kinds: a strongly reactive and a weakly reactive proton. Within the interacting proton model, three different proton site states are defined: the strongly reactive proton state H_1^+, a deactivated proton state H_2^+, and the weakly reactive proton state H_3^+. The strongly reactive proton state H_1^+ catalyzes alkylate formation as well as olefin oligomerization. It deactivates, by deactivating side reactions of the alkylation reaction cycle, to the state H_2^+. Once a proton in the state H_1^+ has a nonreactive H_2^+ proton state as a neighbor, due to the now present negative charge on the zeolite framework in comparison to the deactivation time of the protons, it will nearly instantaneously (faster than a picosecond) convert to a proton state of lower reactivity, H_3^+, that cannot catalyze alkylate formation. Protons in the H_3^+ state will only catalyze alkene oligomerization. They will also deactivate to proton state H_2^+.

Experimental evidence of protons of different reactivity that give only selective alkylation versus alkene oligomerization is taken from the reports of Lercher et al.[10,11] For zeolites of the faujasite structure, they demonstrated that differences in alkylation selectivity between La-promoted X and Y zeolites are related to the location of the reactive proton near La positions in cavities of the zeolite framework.[32,33] Microkinetics simulations of La-containing and non-La-containing zeolites confirm the large selectivity difference of such protons, which can be distinguished by their large difference in ammonia adsorption energy.[26]

In the next section, for later reference, we will present kinetics simulations of deactivation of the alkylation reaction for a single alkylation reactive proton state catalyst model. This will be followed by analogous simulations of the dual interacting proton catalyst model of Figure 2. In the course of deactivation, it generates next to a reactive proton also the less reactive proton. Results will be compared with kinetic simulations of a catalyst model that also contains two kinds of protons with different reactivity, but in this case they do not laterally interact and both are present at the start of the reaction. The highly reactive proton is alkylation selective, and the weakly reactive proton only catalyzes oligomerization.

In the discussion section that follows, we will analyze the nonlinear dynamics of the dual interacting proton model by comparing mean field and stochastic simulations. It will appear that the high coverage of the proton sites with reaction intermediates leads to deviations from the mean field kinetics simulations. Surface percolation of proton dynamics affects the dependence of deactivation on proton concentration. A simple three proton state model, which is not explicitly coupled with kinetics that we introduced previously,[34] will not suffice. The paper is concluded with a short summarizing conclusion section.

2. DEACTIVATION KINETICS OF THE ALKYLATION REACTION

The alkylation reaction network model of the kinetics simulations in this section is shown in Figure 3. The catalyst
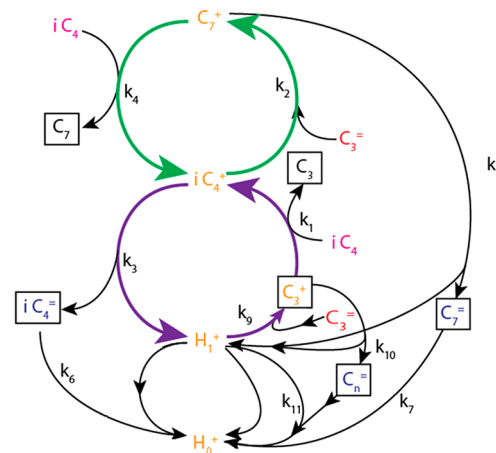
Figure 3. Catalytic reaction cycle of the alkylation reaction including deactivation reaction paths: catalysis by a single reactivity, nonlaterally interacting proton catalyst model. H_1^+ is the reactive proton state, and H_0^+ is the deactivated proton state. The summation of respective concentrations of H_1^+, H_0^+, C_3^+, iC_4^+, and C_7^+ is constant.

model contains only protons of the same reactivity that do not laterally interact. Kinetics of the laterally interacting proton model based on an analogous catalytic cycle will follow in the next section.

The purpose of this section is to show, by modeling deactivation kinetics, the effect of the two deactivation channels on alkylation selectivity. One deactivation channel is the oligomerization of propylene and consecutive deactivation (k_{10} and k_{11}, Figure 3). The other deactivation channel is caused by the deprotonation reactions of carbenium ions iC_4^+ (k_3) and C_7^+ (k_5) and their respective consecutive deactivation reactions (k_6, k_7). In the deprotonation reactions (k_3 and k_5), a proton is regenerated that will reinitiate the initiation reaction cycle by protonation of propylene (k_9).

We will also illustrate in this section the feed-forward relation between the carbenium ion deprotonation reactions (k_3, k_5) and catalyst deactivation through the propylene oligomerization channel (k_{10}).

Another important aspect is the deactivation rate as a function of proton concentration. We will show that, even when protons do not laterally interact, the deactivation rate increases with catalyst surface proton concentration. This happens because surface proton concentration influences the partial $iC_4^=$, $C_7^=$, and $C_n^=$ intermediate product concentrations in the reaction medium.

The reaction starts with all protons in state H_1^+ and stops when protons in state H_1^+ are completely converted into deactivated state H_0^+.

Rate expressions of surface concentrations H_1^+, H_0^+, C_3^+, iC_4^+, and C_7^+ and of reaction intermediates $iC_4^=$ and $C_7^=$ and oligomers $C_n^=$ have been formulated in section SI 1. In the Supporting Information, the details of the solution of the corresponding lumped kinetic equations are discussed where we followed the approach as outlined in ref 35. The lumped elementary reaction rate constants depend implicitly on reagent concentrations. Kinetics simulations correspond to differential
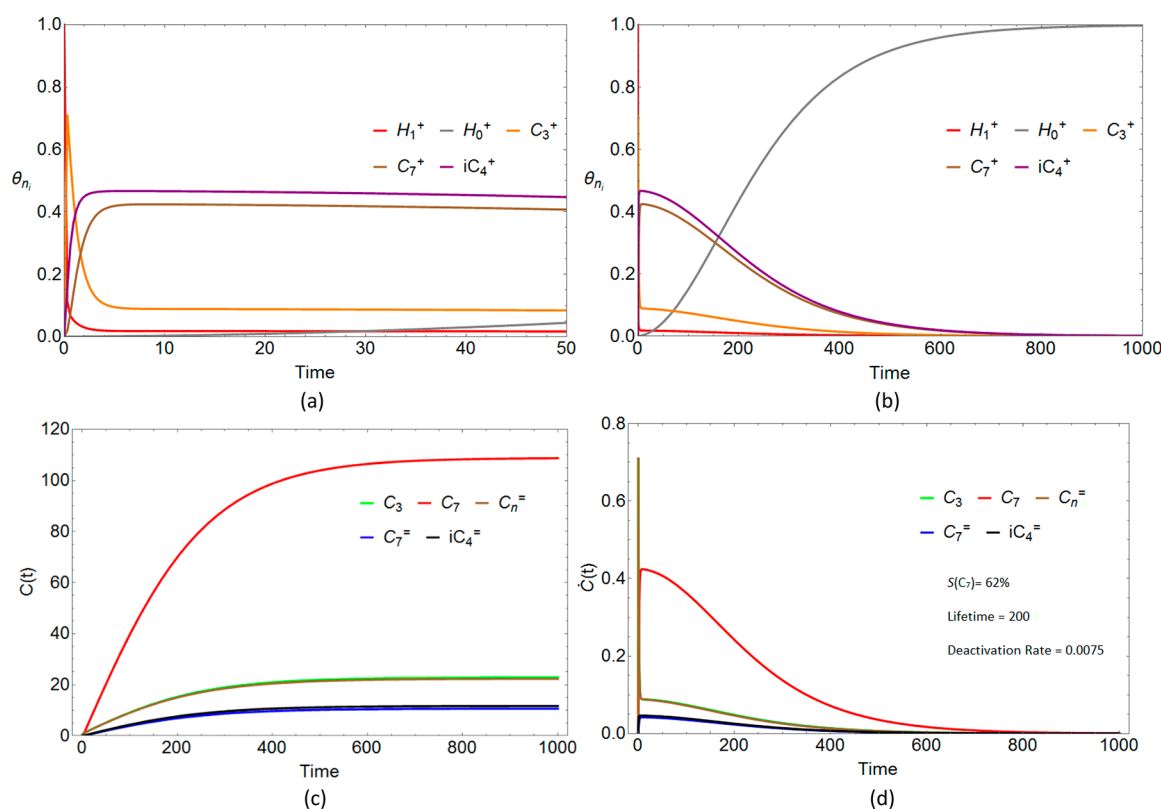
Figure 4. Deactivation kinetics: the case when alkylate production dominates ($k_1 = k_{10} = 1$, $k_2 = k_4 = 1$, $k_3 = k_5 = 0.1$, $k_6 = k_7 = k_{11} = 0.01$, $k_9 = 10$). For kinetic symbols, refer to Figure 3. The rate of hydride transfer is comparable to that of propylene oligomerization. (a) Change in reactant surface concentration at short time scale. (b−d) Longer time scales for the change in surface concentration, product formation, and rate of product formation, respectively, as a function of time. The output concentrations of C_3 and $C_n^=$ and their rates of formation are the same (overlap of green and brown curves in (c) and (d)). In addition, the output concentrations $iC_4^=$ and $C_7^=$ are the same (overlap of black and blue curves (c) and (d)).

conditions, where changes in reactant concentration by reactions can be ignored. The product accumulates as in a batch CSTR reactor, the preferred reactor for alkylation.[10,18] Proton concentration dependence is calculated through definition of dimensionless reaction rate constants as discussed in section SI 2.

Since, as we will see for the dual interacting and noninteracting proton catalyst models, deactivation times of the respective products will be different, accumulated product cannot be used as a measure of product selectivity. A steady-state alkylate selectivity that measures the fraction of propylene incorporation into alkylate can be defined in the intermediate reaction time regime where surface intermediate concentrations are finite and stationary. It is calculated from the expression $S(C_7) = \dot{C}_7 / (\dot{C}_7 + \dot{C}_3 + \dot{C}_7^= + x\dot{C}_n^=) \times 100\%$. Since we do not consider the oligomer length explicitly, x is set equal to 1. The rates of production, $\dot{C}_i$, are deduced from the slopes of the $C_i(t)$ vs t curves. In alkylation catalysis, next to the selectivity, catalyst lifetime is usually the measure by which the activities of different catalysts are compared. The catalyst lifetime is defined as the time when the rate of production starts to decline exponentially. The catalyst decline rate is defined as the inverse slope of the logarithmic plot of $\dot{C}(t)$ vs t when the atalyst deactivation rate has become exponential. The unit of time is k_1^{-1}, which is maintained the same in the simulations. In the respective figures (or legends), we mention alkylation selectivites as well as lifetimes and deactivation rates.

We will compare kinetics simulations when alkylate is the major product and when instead oligomerization of alkenes

dominates. The differences are defined by respective default elementary reaction rate parameters that remain the same throughout the paper, unless mentioned specifically.

First-principles microkinetics simulations based on quantum chemically calculated elementary reaction rate data representative for these two cases are available.[26] In these simulations, faujasite zeolites with reactive and less reactive protons were compared. The default reaction rate parameters selected in the kinetics simulations of this paper have been chosen to give approximate agreement with the data of the microkinetics simulations. The default reaction rate constant of the initiating hydride transfer reaction k_1 (Figure 3), which is scaled to 1, has been chosen to be equal to the rates of the reactions of the propagation cycle ($k_1 = k_2 = k_4 = 1$). Reaction rate constants of deprotonation of iC_4^+ and C_7^+ are chosen 1 order of magnitude less ($k_3 = k_5 = 0.1$). Reaction rate constants of proton deactivation by alkenes or alkene oligomers again are chosen 1 order of magnitude smaller ($k_6 = k_7 = k_{11} = 0.01$). The reaction rate of propylene protonation to form intermediate carbenium ion is fast ($k_9 = 10$). k_{10}, the lumped elementary reaction rate constant of reactant alkene oligomerization, has been chosen to vary. For high alkylation selectivity, k_{10} is chosen equal to k_1, the elementary reaction rate constant of hydride transfer. For the low alkylation selectivity case, k_{10} is chosen as 10 times k_1. This increased reaction rate constant can be considered to be due to an increased reactant concentration of propylene. There is no k_8. This is reserved for the elementary reaction rate constant of proton dynamics in the dual site interacting proton catalyst model to be discussed in section 3.
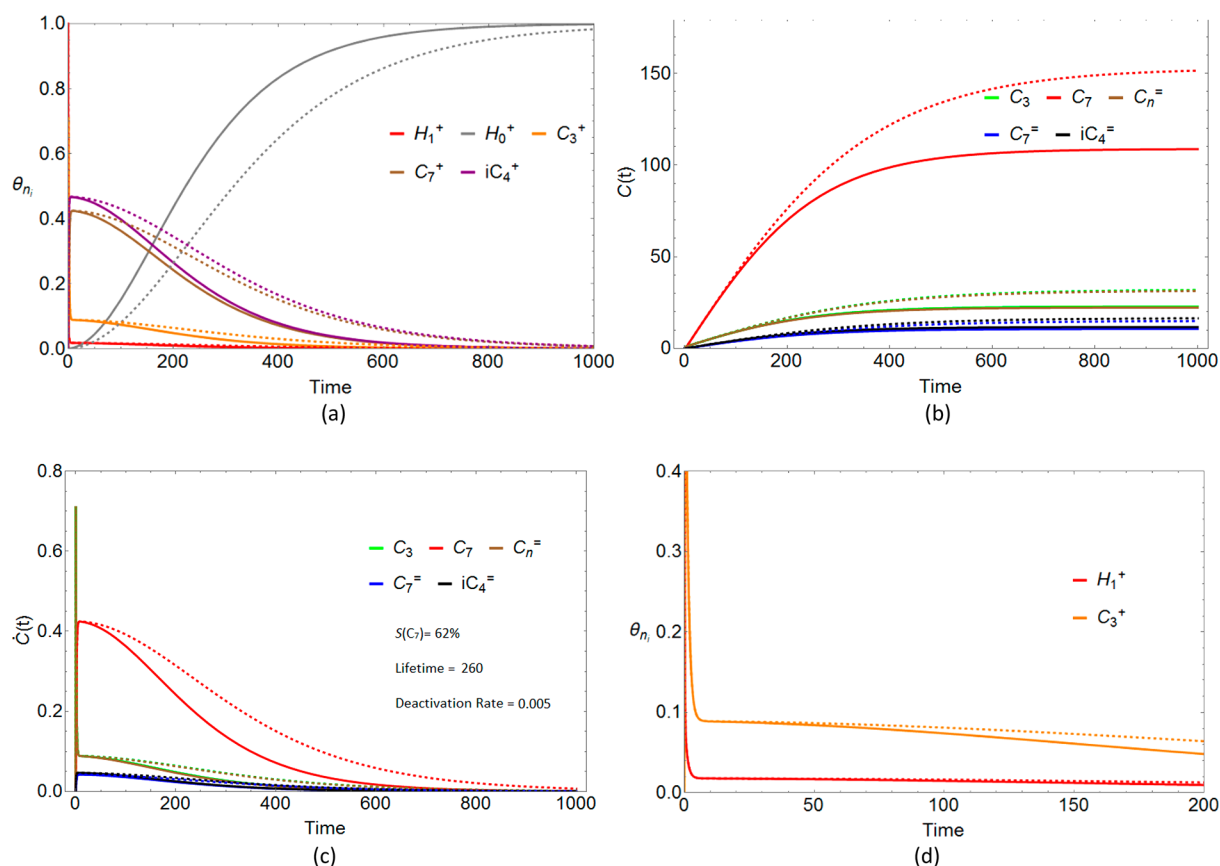
Figure 5. Effect of proton surface concentration on catalyst deactivation. The same reaction rate parameters are used as in Figure 4, the case of dominant alkylate production. A comparison of deactivation rates is made with a proton density reduced by half (broken curves). (a) Change in reactant surface concentration with time. (b, c) Product formation and rate of product formation normalized per proton with time. (d) Initial H_1^+ and C_3^+ surface concentrations as a function of time.

2.1. Deactivation Kinetics for High and Low Alkylation Selectivity.
We will compare deactivation kinetics when alkylation selectivity is relatively high and low. It will mainly depend on the reaction rate ratios of hydride transfer reactions (k_1 and k_4) versus the reaction rates of propylene oligomerization (k_{10}) and deprotonation (k_3, k_5), respectively. We will also consider the effect of proton concentration on selectivity and deactivation rate of the reaction.

In Figure 4, we consider the case where alkylate production dominates. We select the rate of reaction initiation by hydride transfer to the C_3^+ cation to be comparable to the rate of olefin addition ($k_1 = k_{10} = 1$). For this case, Figure 5 compares deactivation rate as a function of proton concentration. Figure 6 gives the results of kinetics simulations where the elementary reaction rate of olefin oligomerization is much faster ($k_1 = 1$, $k_{10} = 10$).

For high alkylation selectivity, the relative concentration of reactant propylene has to be low in comparison to that of isobutane. Figure 4a,b shows surface coverage in the initiation and deactivation time regimes, respectively. Product distributions and their respective rates of deactivation are shown in Figure 4c,d.

In Figure 4 and later figures, we will plot the surface concentrations of reaction intermediates, θ_{ni}, the amount of product produced per unit proton, $C(t)$, and the rate of change of product produced also normalized per unit proton, $\dot{C}(t)$. Figure 4a shows rapid initial proton consumption and overshoot of C_3^+ formation. After a relatively short time, C_3^+ intermediate

formation is overtaken by iC_4^+ and C_7^+ formation and a steady-state situation evolves. The steady-state alkylate selectivity is mentioned in the legend and equals 62%. Figure 4c illustrates the accumulation of reaction products with time. As the catalyst starts to deactivate, the accumulated product reaches its maximum. In this case, steady-state selectivity and accumulated product selectivity are similar. In the dual interacting and noninteracting proton catalyst models that we will discuss in the section 3, this will not be the case, since the deactivation times of the different products will be different.

Figure 4b,d illustrates the rate of catalyst deactivation that starts at time 40 in the simulations. Then the deactivated proton state H_0^+ starts to appear in Figure 4b. The main reaction product is C_7 alkylate. The next coproducts are propane C_3 and propylene oligomer $C_n^=$, followed by $iC_4^=$ and $C_7^=$ formation.

The lifetime of the catalyst is 200 time units as deduced from the logarithmic plots of product rates of formation, when the slope starts to deviate from zero (see Figure S1a in section SI 1). When the deactivation rate has become exponential, the catalyst deactivation rate becomes equal to 0.0075 time^{-1}. In alkylation kinetics, differences in steady-state selectivity multiplied by catalyst lifetime are the determinants that define their productivity.

Whereas the elementary reaction rate constant of propylene oligomerization is 10 times larger than the deprotonation reaction rate constants, in the simulations the respective apparent reaction rates are nearly the same (the factor of 2 difference observed in Figure 4c,d is derived because protons are
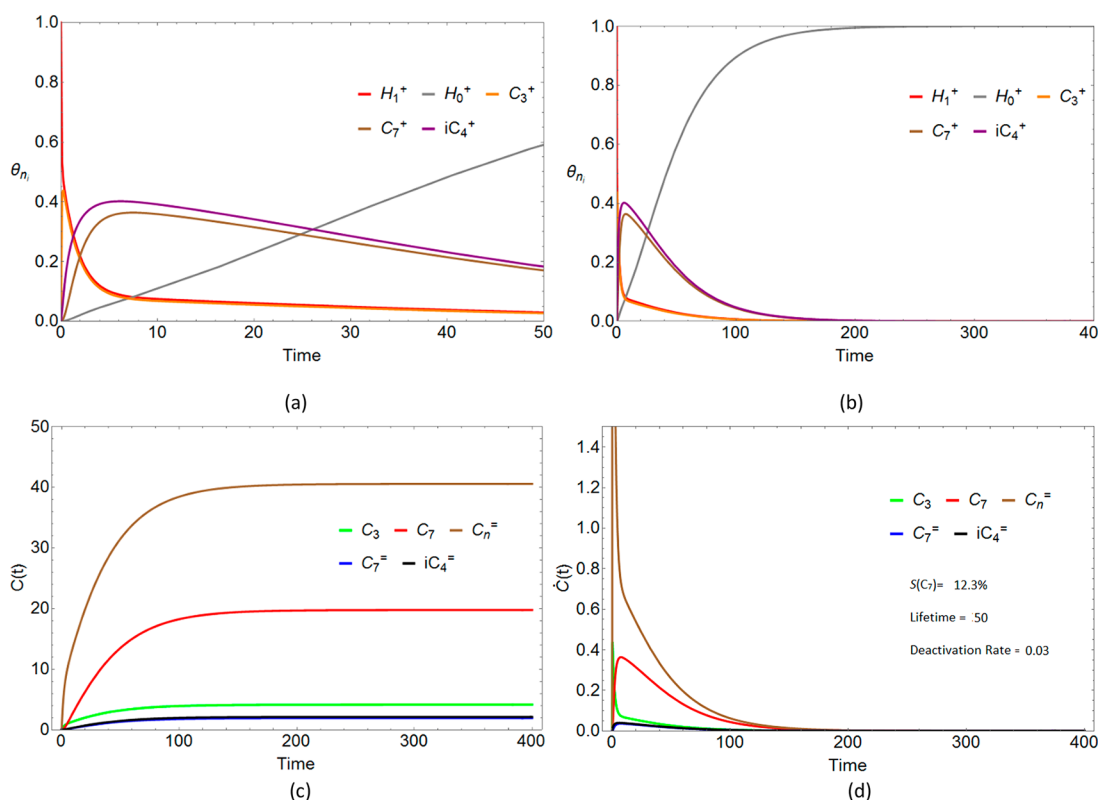
Figure 6. Deactivation kinetics: the case of low alkylation selectivity. The rate of propylene oligomerization is fast in comparison to that of hydride transfer ($k_1 = 1, k_{10} = 10, k_2 = k_4 = 1, k_3 = k_5 = 0.1, k_6 = k_7 = k_{11} = 0.01, k_9 = 10$). (a) Rate of proton consumption and change in surface concentration on a short time scale. (b−d) Longer time scales for the change in surface concentrations, product formation per unit proton, and rate of product formation per unit proton, respectively, as a function of time.

generated by the two deprotonation reaction iC_4^+ and C_7^+). The reduced relative rate of the oligomerization reaction is because oligomerization has to compete with hydride transfer in the initiation reaction.

Experiments of the alkylation reaction of *n*-butene and isobutane[36] show, in the regime of high alkylation selectivity, coreaction products due to addition of butenes to the C_8 olefins. They can be considered signatures of the deprotonation reaction of the intermediate carbenium ions.

It is interesting to compare the variation in decay time with initial concentrations of protons. Although the protons do not laterally interact, proton concentration affects the selectivity and deactivation rate of the reaction, because reaction intermediates will have different concentrations in the reaction medium. This is illustrated in Figure 5.

In the steady-state regime, respective selectivities are the same but deactivation times are different. This makes the selectivity of accumulated products different. In Figure 5a, the delay of deactivation when surface concentration is reduced is illustrated from the different time dependences of the surface intermediate. As shown in Figure S1b in section SI 1, a reduction in proton density by half increases the catalyst lifetime time from 200 time steps to 260 time steps. The rate of decline (see Figure 5c) decreases by a factor of 30% (the alkylation deactivation rate is 0.005 time^{-1}). When the proton density was reduced by half (Figure 5b) a higher product formation rate per proton occurs. This happens because in the initiation cycle at reduced proton density there is less deactivating propylene oligomerization. In Figure 5d, this is reflected in the increased C_3^+ surface concentration when the proton density is reduced.

When the proton density is decreased, two competing phenomena occur. First, the product formation per unit surface area becomes reduced because of less reactive sites. Then the deactivation of H_1^+ by readsorption of oligomers (k_6, k_7, k_{11}) produced via the reaction steps k_3, k_5, and k_{10} also becomes less.

Figure 6 shows the results of kinetic simulations when the reaction rate of propylene oligomerization is large in comparison to that of the hydride transfer reaction rate ($k_1/k_{10} = 0.1$). Now the rate of propylene oligomer formation, $C_n^=$, is high in comparison to that of alkylate C_7 production and the rate of deactivation has become substantially faster. Steady-state alkylate selectivity is calculated where the surface coverage of the reaction intermediate is maximum. It has dropped to 12.3%. The catalyst lifetime equals 50 time steps, and the deactivation rate becomes 0.03 time^{-1}.

The kinetics simulations apply to a batch reactor and differential conditions where the reactant concentration does not change during the reaction. Experimentally, the preferred reactor for the alkylation reaction is a CSTR, because the reactant concentration in it is uniform and the reactant alkene concentration can be kept low. When the reaction is executed with initial excess isobutane and 100% conversion of reactant alkene,[18] the alkylation selectivity is high and the rate of catalyst deactivation is relatively slow. The catalyst lifetime can be on the order of 10 h or more. Then the reaction rate of hydride transfer is large in comparison to the apparent reaction rate of alkene oligomerization and intermediate carbenium ion deprotonation. The kinetics can be considered similar to that shown in Figure 4.

Of course then, as long as in the experiment conversion of propylene remains 100%, no change in propylene conversion is
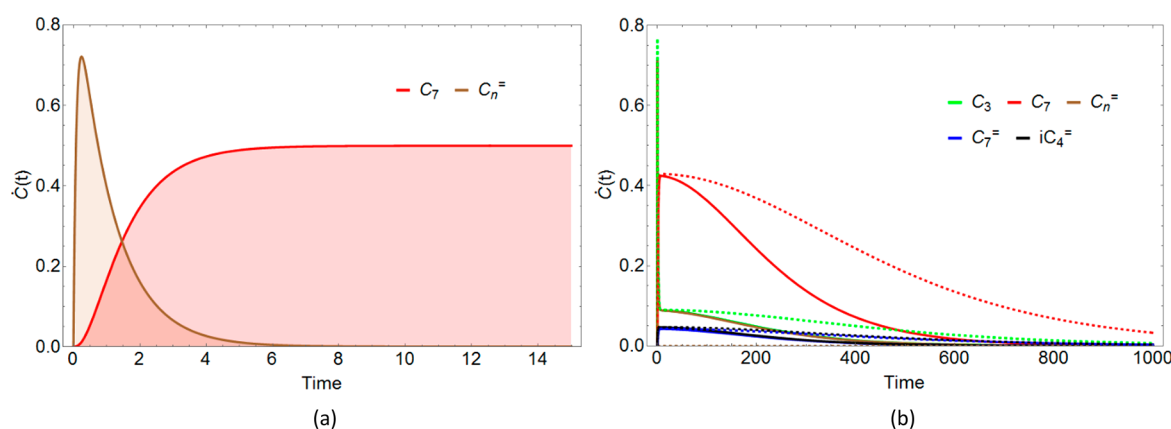
Figure 7. Feed-forward relation between rates of carbenium ion deprotonation and propylene oligomerization with default parameters for dominant alkylate production ($k_1 = k_2 = k_4 = 1$, $k_3 = k_5 = 0.1$ $k_{11} = 0.01$, $k_9 = 10$). (a) Time dependence of rate of change of products when reaction rates of deprotonation of carbenium ions in the propagation reaction cycle are zero ($k_6 = k_7 = 0$, $k_{10} = 1$; steady state $S(C_7) = 100\%$) (b) Comparison of two cases. The solid lines show the rate of product formation similar to that in Figure 4, where both deactivation channels contribute to catalyst deactivation. The dashed lines show the rate of product deactivation when the deactivation channel through propylene oligomerization is closed ($k_6 = k_7 = 0.01$, $k_{10} = 0$; steady state $S(C_7) = 75\%$).

observed. However, the rates of alkylate and light alkane production decrease gradually and there is a gradual increase of oligomers due to the deprotonation reaction.[8,10,11] Once alkene conversion drops below 100%, then due to the suddenly increased alkene concentration, the relative rate of alkene oligomerization increases sharply, alkylate selectivity drops sharply, and the rate of catalyst deactivation increases.[10,18] Now the kinetic simulations of Figure 6, with the increased rate constant of propylene oligomerization (k_{10}), apply.

2.2. Feed-Forward Relation between the Deprotonation and Oligomerization Reactions. As illustrated in Figure 1, catalyst deactivation goes through two deactivation channels. One deactivation channel competes with the initiation reaction cycle. Then propylene oligomerization competes with the hydride transfer reaction of isobutane with propyl cation. The other deactivation channel results from the deprotonation reactions of iC_4^+ and C_7^+. This reaction is a parasite on the propagation reaction cycle. At the same time, it reinitiates the initiation reaction cycle. This can be demonstrated by a simulation where the elementary reaction rate constants of deprotonation k_6 and k_7 are put equal to zero (see Figure 7a).

Figure 7a shows a short transient period of initial propylene oligomer formation, which is rapidly taken over by constant production of alkylate with 100% selectivity. After the initial transient period, the initiation reaction cycle is taken over by the propagation reaction cycle that cannot deactivate because of the absence of the deprotonation reactions.

The feed-forward relation between deprotonation and propylene oligomerization is illustrated in Figure 7b. In this figure, a comparison is made between the two deactivation channels by suppression of the propylene oligomerization reaction. This case is compared with both deactivation channels being operational (default case). This illustrates that when alkylation selectivity is high the dominant deactivation channel is carbenium ion deprotonation. The catalyst lifetime is not significantly affected. It is only reduced by half and the rate of catalyst deactivation is increased by a factor of 2 when both deactivation channels contribute. Alkylation selectivity is slightly higher when propylene oligomerization is suppressed.

3. DUAL INTERACTING PROTON CATALYST MODEL

Here we will compare deactivation kinetics according to the dual interacting proton catalyst model of Figure 2 with catalyst deactivation by a dual noninteracting proton catalyst model. This dual noninteracting proton catalyst model contains two kinds of protons of different reactivities as the dual interacting proton model, but these protons have no lateral interaction. They are permanently present during the reaction.

In the dual interacting proton catalyst model, the three proton states H_1^+, H_2^+, and H_3^+ are defined. Proton states H_1^+ and H_3^+ are strongly reactive and weakly reactive, respectively, and proton state H_2^+ is the deactivated proton state. Proton state H_1^+ is converted to proton state H_3^+ when a proton is present on a neighboring site in the deactivated proton state H_2^+. Protons H_1^+ produce alkylate as well as alkene oligomers. Protons H_3^+ only catalyze propylene oligomer formation. In the dual interacting proton model, at the start of the reactions only protons in the state H_1^+ are present.

In contrast to the dual noninteracting proton catalyst model, protons in the reactive proton state H_1^+ are not converted into protons of the weakly reactive proton state H_3^+. Protons in respective proton states H_1^+ and H_3^+ are present from the start of the reaction. Different from the dual interacting proton catalyst model, their deactivated states will not affect the reactivity of protons in either proton state H_1^+ or H_3^+.

The comparison of the two catalyst models is relevant, since it has been suggested[10,11] that the experimentally observed delayed production of alkene oligomerization is due to the additional presence of weakly reactive protons that only catalyze alkene oligomerization. This continues after the decline of alkylate production, which is catalyzed by strongly reactive protons.

Here we will show that an increase in oligomer production once alkylate production has declined is only consistent with a laterally interacting proton catalyst model. We will also see that alkylate production has a reduced lifetime when it is catalyzed by the dual interacting proton catalyst model in comparison with the lifetime when isolated protons catalyze the reaction. This is due to a decrease in neighbor deactivated proton sites next to it. In section 4, the effect of surface vacant proton sites on catalyst lifetime will be discussed in more detail.

Figure 8 shows the catalytic reaction cycle of the dual interacting proton catalyst model. Parts of the elementary

Figure 8. Catalytic reaction cycle of the alkylation reaction of propylene and isobutane according to the dual interacting proton catalyst model. Conservation of surface species: $H_1^+ + H_2^+ + H_3^+ + C_3^+ + C_3^{+\prime} + iC_4^+ + C_7^+ = 1$.

reactions are similar to those in Figure 3, the catalytic reaction cycle of the single proton case, except that proton state H_1^+ is converted to the less reactive state H_3^+, when a deactivated proton state H_2^+ becomes a neighboring site. Since this conversion has an electronic cause, the corresponding rate constant k_8 is fast in comparison to chemical reaction rates. Its default value is chosen as fast such that the kinetics is not affected by its further increase. The pr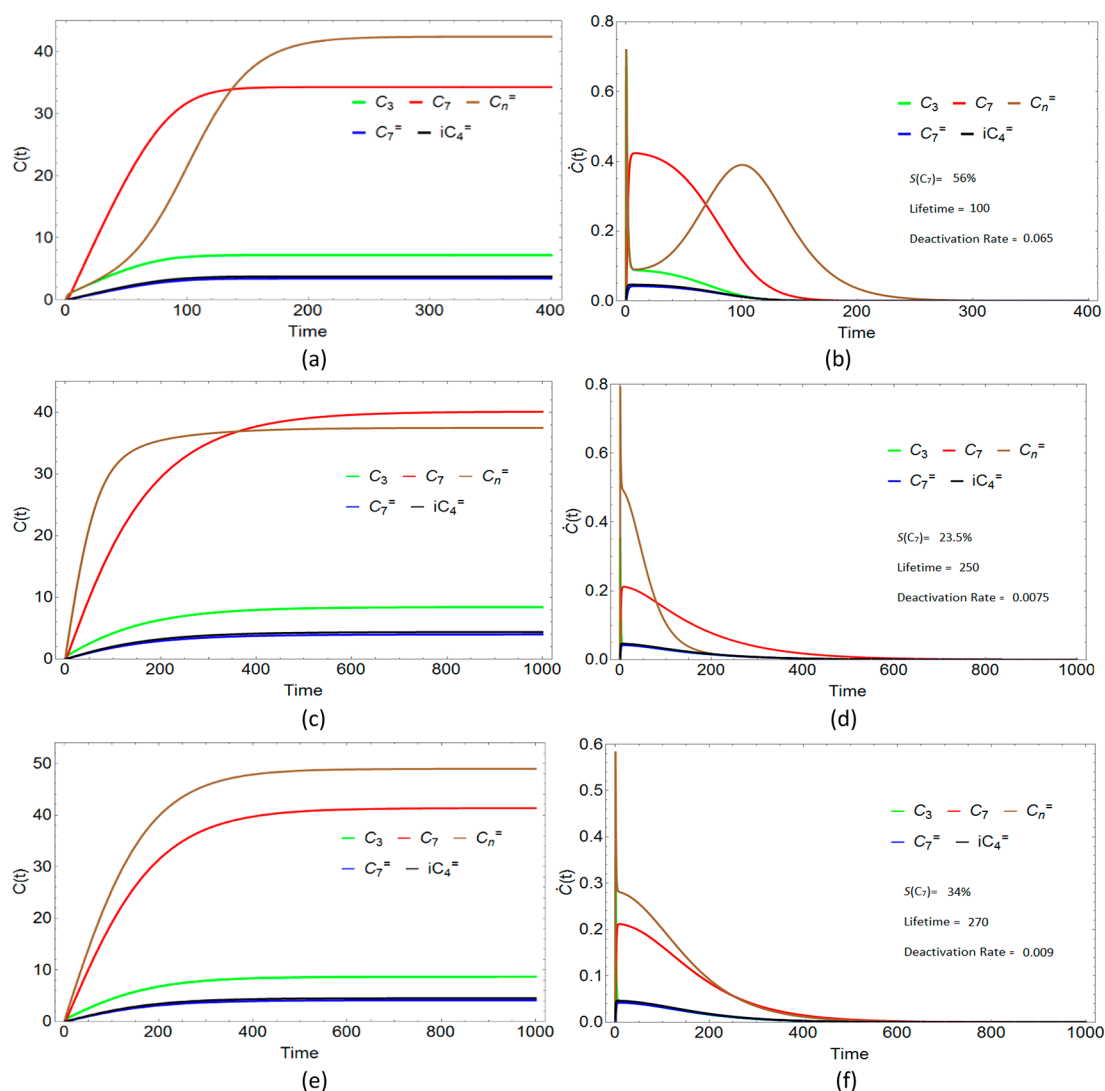oton state H_3^+ will not initiate the alkylation reaction but only catalyze the oligomerization reaction of propylene. Default parameters of the reaction rate constants of oligomerization by protons in the state H_3^+ are

chosen the same as those of oligomerization by the protons in the state H_1^+.

The ordinary differential equations that calculate the time dependence of the dual interacting proton catalyst model are solved in a fashion analogous to that for the kinetics equations that correspond to the reaction cycle of the single proton reactivity model of Figure 3. Details are given in section SI 3.

Figure 9 shows the reaction cycles that correspond to the dual noninteracting proton catalyst model. It shows two independent reaction cycles. One reaction cycle is the same as in Figure 3, and the other concerns the oligomerization of propylene only and the corresponding proton deactivation. The solutions of the corresponding kinetics equations are given in section SI 4.

In Figure 10, the deactivation patterns of the dual interacting proton catalyst model and the noninteracting proton catalyst model are given. For the dual interacting proton catalyst model, in Figure 10a,b changes in production formation and rate of product deactivation are shown with time. Default kinetic parameters have been chosen that, for the single proton catalyst model, give high alkylate selectivity.

Different from the single proton catalyst model, now deactivation times of reaction products are different. The selective alkylate production lifetime is now 100 time steps, 0.5 times shorter, and the decline rate of alkylate production 0.065 time^{-1}, 8.33 times faster, in comparison to those of the single proton catalyst model. After the decline of selective alkylate production, there is an overshoot of oligomer production. This overshoot of oligomer production is also apparent from Figure 10b, which shows the time dependence of production rates of products.

Similar to the case in alkylation batch experiments, this catalyst model will only show high alkylate selectivity when the reaction is stopped in time before oligomer overshoot production sets in. Steady-state selectivities are mentioned in the legends. The steady-state alkylate selectivity is now 56%, which is, as expected, slightly less than that for the single proton catalyst model.

As we will explain in detail in section 4, enhanced deactivation of alkylate production and overshoot of oligomer production derive from the rapid conversion of proton state H_1^+ to the less reactive proton state H_3^+ once a deactivated proton state H_2^+ appears next to it. Protons in proton state H_3^+ are initially absent

Figure 9. Dual noninteracting proton catalyst model mechanism. Protons of the two catalyst cycles are not shared, but oligomer production $C_n^=$ interacts with both reaction cycles. Protons in the state H_1^+ catalyze alkylation and oligomerization, and protons in the state H_3^+ only catalyze oligomerization. Conservation of surface species: $H_1^+ + H_2^+ + iC_4^+ + C_7^+ + C_3^+ = 1/2$, $H_2^+ + H_3^+ + C_3^{+\prime} = 1/2$.

Figure 10. Comparison of deactivation kinetics of the dual interacting proton catalyst model with that of the dual noninteracting proton catalyst model. Default kinetics model parameters are the same as those for high alkylate selectivity in the single proton catalyst model ($k_1 = 1$, $k_2 = k_4 = 1$, $k_3 = k_5 = 0.1$, $k_6 = k_7 = 0.01$, $k_8 = 10$, $k_9 = k_9' = 10$, $k_{10} = 1$, $k_{10}' = 1$, $k_{11} = k_{11}' = 0.01$). (a, b) Kinetics of dual interacting proton catalyst model: (a) product formation normalized per proton; (b) rate of product deactivation normalized per proton as a function of time. (c−f) Kinetics of dual noninteracting proton catalyst model (the concentrations of $iC_4^=$ (black line) and $C_7^=$ (blue line) always overlap): (c) product formation normalized per proton as a function of time; (d) rate of product formation normalized per proton as a function of time; (e, f) product formation per proton and rate of product formation per proton with protons H_3^+ less reactive ($k_{10}' = 0.5$; $k_{11}' = 0.005$). The C_3 formation rate overlaps with $iC_4^=$ and $C_7^=$ rates of formation after an initial spike. (g) Comparison of deactivation rates of alkylate production of the single reactivity proton catalyst model and those of the dual noninteracting proton catalyst model (comparison is done normalizing the data of dual interacting proton model on the density of highly reactive protons, with the same default parameters).

in the dual interacting proton catalyst model. Their later formation is the reason for the overshoot in oligomerization production after alkylation decline. In Figure S3, complementary to Figure 10, the time evolution of surface intermediates is shown. The product evolution closely follows the occupation of H_1^+ and H_3^+ protons.

Figure 10c,d shows, for the same elementary reaction rate default parameters, comparable data for the dual noninteracting proton catalyst model. In comparison to the proton concentration in the dual site interacting proton catalyst model, in this figure, the concentrations of respective proton states H_1^+ and H_3^+ have been initialized to cover half the surface each.

As we have explained in section 2, this reduction in proton density causes the deactivation of alkylate production to be delayed by a factor of 1.3 in comparison to the single proton case (Figure 5c).

The now high initial relative rate of oligomer production is dramatic in comparison to that in the other two proton catalyst models. It is due to the high oligomerization rate of the H_3^+ protons. In the dual noninteracting proton catalyst model, different from the other catalyst models, oligomerization by the H_3^+ protons does not compete with the hydride transfer reaction. The lifetime of alkylate production is 250 time steps, which is slightly longer than that of the single proton catalyst model of 200 time steps but the lifetime of oligomer production has decreased to 130 time steps. Now, after a decline of oligomerization, alkylate production dominates. In comparison to the single proton catalyst model, the steady-state alkylate selectivity has decreased by 61%. Because of its longer lifetime,

accumulated alkylate production is higher than that of oligomer production.

Kinetics as shown in Figures 10c,d will sensitively depend on the rate of deactivation of the H_3^+ protons by the oligomer molecules. The oligomerization catalysis by the weakly reactive protons in the proton state H_3^+, which are not able to catalyze alkylation, should be slower than that of the H_1^+ protons that are able to catalyze this reaction. Such a decreased rate of deactivation of the less reactive protons H_3^+ is consistent with their known lower rate of propylene oligomerization. Sarazen et al.[37] indicate a decrease by at least a factor of 10 in oligomerization rate when the reactivity of highly reactive and less reactive protons in faujasite zeolite are compared.

Figure 10e,f presents oligomer product formation and deactivation rates of deactivation, when accordingly their respective reaction rate constants catalyzed by protons in proton state H_3^+ (k_{10}', k_{11}') are reduced by half. In comparison to Figure 10c,d, now steady-state alkylate selectivity increases, but oligomer production also dominates at longer times. The lifetime of oligomer production is 260 time steps, and its deactivation rate of 0.01 time^{-1} is now close to that of alkylation (0.009 time^{-1}). Importantly, different from the dual interacting proton catalyst model, beyond deactivation of alkylation, the slope of oligomerization rate change is always negative.

In the dual noninteracting proton catalyst model, the reactivity of proton states H_1^+ and H_3^+ is coupled through deactivation by oligomers that are produced by both proton states. When it is normalized to the same initial H_1^+ proton concentration, the alkylation lifeitme of the dual noninteracting proton catalyst model is reduced by 5% in comparison to the single proton catalyst model.

In this section, we presented simulations with default elementary reaction rate constants that give, for the single proton catalyst model, relatively high alkylate selectivity. In section 4, for the dual interacting proton catalyst model, we will also analyze simulations when alkylate selectivity is low.

This section has provided evidence that alkylate production lifetime is longest when only reactive protons H_1^+ are initially present and these protons are isolated. The deactivation rate increases by 1 order of magnitude when lateral interactions between protons H_1^+ are present. Because of the generation of weakly reactive protons H_3^+, later in time, delayed production of oligomers occurs after a decline of alkylate production.

Different from the dual interacting proton catalyst model, the dual noninteracting proton catalyst model has a lower initial selectivity of alkylate production in comparison to that of oligomer formation. As previously mentioned, this selectivity difference is due to the apparent higher rate of oligomer formation by the also initially present protons H_3^+ that cannot catalyze alkylate formation.

In the next section, we will analyze the proton dynamics that is fundamental to the kinetic differences induced by the lateral interactions of the protons. The rate of alkylate production follows the dynamics of protons H_1^+, and the rate of oligomer production follows the dynamics of protons H_3^+.

4. DISCUSSION OF DEACTIVATION KINETICS

Kinetics modeling, discussed in section 3, has demonstrated that deactivation kinetics changes nonlinearly when protons interact laterally. In the section 4.1, we will analyze the dynamics of a three proton state model that shows deactivation dynamics similar to that discussed above for the dual site interacting proton catalyst model, but without coupling to the full reaction kinetics scheme of Figure 3. The advantage of this three proton state model is that analytical solutions of its dynamics can be found. We will use nonlinear dynamics to deduce the relation between the rates of deactivation of protons in respective H_1^+ and H_3^+ states and their rate of interconversion.

In section 4.2, we will return to the full dual interacting proton catalyst model. We will compare stochastic simulations with solutions of the corresponding mean field equations. The stochastic simulations will be used to study deactivation kinetics of laterally interacting protons as a function of proton coordination.

4.1. Dynamics of the Three Proton State Model. In the first part of this section, we will present a mean field analysis of a three proton state dynamics model that simulates deactivation without explicit consideration of the full kinetics of the alkylation reaction. The section will be concluded with a comparison of mean field and stochastic results that includes an analysis of the dependence on proton coordination to other protons.

The mean field ordinary differential equations that describe the time evolution of probabilities n_i of the respective proton states H_i^+ are given by eqs 1a–1c:

$$\frac{dn_1}{dt} = -k_{12}n_1 - mk_{13}n_1n_2 \tag{1a}$$

$$\frac{dn_2}{dt} = k_{12}n_1 + k_{32}n_3 \tag{1b}$$

$$\frac{dn_3}{dt} = -k_{32}n_3 + mk_{13}n_1n_2 \tag{1c}$$

The rate constants k_{12} and k_{32} refer to the respective proton deactivation rates of proton states H_1^+ and H_3^+. As in the dual site interacting proton catalyst model, proton state H_1^+ represents the reactive proton state that catalyzes the alkylation reaction and proton state H_3^+ represents the proton state that only catalyzes propylene oligomerization. The rate constant k_{13} is the rate of conversion of proton state H_1^+ to proton state H_3^+ when it gets as a neighbor the deactivated H_2^+ proton state. Since the rates of local surface atom rearrangement and electronic changes will be several orders of magnitude faster than the deactivation rates of proton states H_1^+ and H_3^+, respectively, one expects k_{13} to be large in comparison to k_{12} and k_{32}. m in eq 1a is the number of neighbors of a proton.

If in eq 1a k_{13} is set equal to zero, eqs 1a and 1c decouple and the probabilities n_i correspond to that of the dual noninteracting proton catalyst model. Each proton will decay exponentially with decay constants $1/k_{12}$ and $1/k_{32}$, respectively.

In the simulations of the dual interacting proton catalyst model shown in Figure 10a,b, we observe a delayed oligomer production after alkylation production has declined. Since this reflects the respective dynamics of protons H_1^+ and H_3^+, we are interested to know for which relationship of the rate constants in eq 1a, deactivation of protons in state H_1^+, that catalyze alkylation, occurs quickly and protons in state H_3^+ that only catalyze oligomerization remain active after deactivation of the H_1^+ protons.

The condition for this to happen is that proton state probability n_3 crosses state probability n_1 (see Figure 11). One can deduce an approximate condition that is given in eq 2 (for the proof, refer to section SI 5.2):

$$k_{12} + 2mk_{13} > k_{32} \tag{2}$$
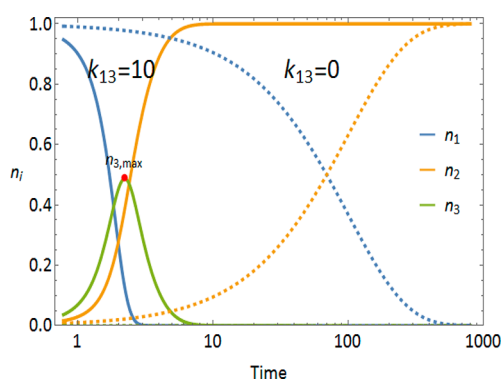
Figure 11. Dynamics of the three proton state model. Rate parameter values: $k_{12} = 0.01$, $k_{32} = 1.0$. Comparison of time evolution of proton state probabilities n_i of protons H_i^+, respectively, with strong coupling of the protons ($k_{13} = 10.0$, solid lines) and absence of coupling of the protons ($k_{13} = 0$, dashed lines). The time evolution of respective proton states H_1^+, H_2^+, and H_3^+ are simulated with rate constants such that state probability n_3 crosses state probability n_1. This is, within dual interacting proton catalyst model, the condition of delayed oligomer production (see Figure 10b).

According to this relation, when the conversion rate of proton state H_1^+ to proton state H_3^+ is fast, after decay of alkylation, oligomer formation still increases and it decays later. This delay becomes independent of k_{13} when it exceeds a maximum value.

When the intrinsic rate of deactivation of proton in state H_1^+ (k_{12}) is small, a high rate of conversion of proton state H_1^+ to proton state H_3^+ (strong coupling between the protons; $2mk_{13}$) is necessary to overcome the rate of deactivation of the protons in state H_3^+ (k_{32}). A low rate of proton state H_1^+ deactivation implies dynamics that corresponds to high initial alkylate selectivity. As Figure 10c illustrates, when proton states are decoupled, the rate of deactivation of proton H_3^+ (reflected in the deactivation rate of oligomerization) is greater than the deactivation rate of proton state H_1^+ (reflected in the deactivation rate of alkylation). The proton dynamics that corresponds to the kinetics of dual interacting proton catalyst model kinetics of Figure 10b and dual noninteracting proton catalyst model of Figure 10d, both calculated with the same default parameters, is shown in Figure 11.

Figure 11 shows the proton dynamics of the interacting three proton catalyst model, where the condition of eq 2 is satisfied. A comparison is made with the independent proton dynamics.

The rate constant of proton state H_1^+ deactivation has been chosen to be slower than that of proton state H_3^+. The strong coupling between proton states causes, in the coupled system, deactivation of proton state H_1^+ to be faster than that of proton state H_3^+. Slow exponential decay of proton state H_1^+ is converted into fast nonexponential accelerated decay. This is even the case when the deactivation rate constant of reactive proton state H_1^+ ($k_{12} = 0.01$) is initially slower than that of the less reactive proton state H_3^+ ($k_{32} = 1$).

For a detailed nonlinear dynamics analysis[38] of eqs 1a, where four different deactivation rate regimes are identified, we refer to section SI 5. It appears that only one deactivation rate regime shows dynamics as found in Figure 11.

Before returning to the full kinetics of the alkylation reaction, we present stochastic simulations[39−41] of the dynamics of the three proton state model and compare these with the mean field solutions.

4.1.1. Stochastic Solution of the Three Proton State Model: Proton Coordination Dependence. In the stochastic simulations, the protons are considered to be located on a lattice as indicated in Figure 12. A proton can have as a neighbor another
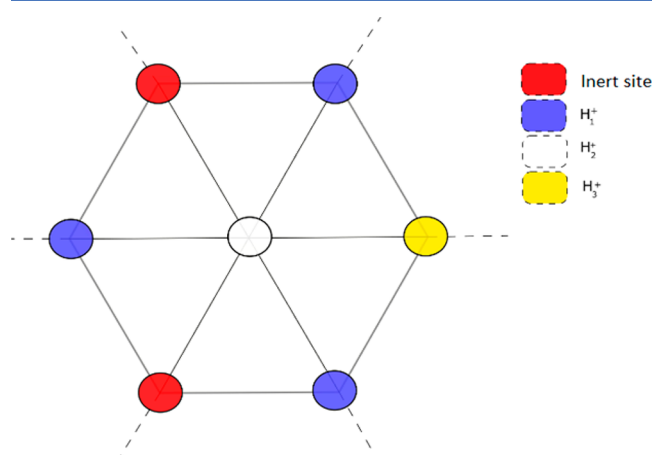
Figure 12. 2D lattice representation of the laterally interacting three proton catalyst model.

proton in the same state. In addition, we will consider also the possibility of inert site vacancies that will have state probability n_4. Method details on the stochastic simulations are provided in section SI 5.3.

Stochastic simulations and mean field equations give very similar results except for the chemically relevant case of Figure 11 (see section SI 5). We will limit the discussion here to this case, where proton state H_3^+ deactivation is delayed beyond deactivation of proton state H_1^+. As we will see, the difference between the mean field and stochastic simulations is due to pattern formation of the respective proton states in the latter. When the mean field approximation is used, as in section 4.1, the implicit assumption is made that the distribution of proton states is uniform. Stochastic simulations make the conversion of proton states H_1^+ to proton states H_3^+ faster. The decay of proton state probability n_1 is faster, and there is more delay of proton state probability n_3.

Here, we will show this for the three proton state model. In section 4.2, the consequences of this pattern formation will be investigated. Then, in simulations, proton dynamics and kinetics are coupled.

Mean field and stochastic simulations of the respective proton states are shown in Figure 13. The dashed lines show the time evolution for the stochastic case. The solid lines give the corresponding mean field calculated values. We compare a surface without vacancies ($n_4 = 0$) with two surface configurations in which vacancies are present ($n_4 = 0.3$, $n_4 = 0.7$).

Significant differences between mean field solutions and stochastic simulations can be observed in the simulations of Figure 13. For convenience of comparison, they have been done with same parameter values as used in Figure 11. Stochastic simulations slow the rates of deactivation. The differences in the fast decay time of proton state H_1^+ and the delayed deactivation time of proton state H_3^+ decrease.

When vacancy concentration n_4 increases, the decreased coupling of proton states H_1^+ and H_3^+ causes the decay rate of proton states H_1^+ and deactivation delay of proton states H_3^+ to become less. This confirms the previous conclusion that the alkylation deactivation rate becomes less when protons become
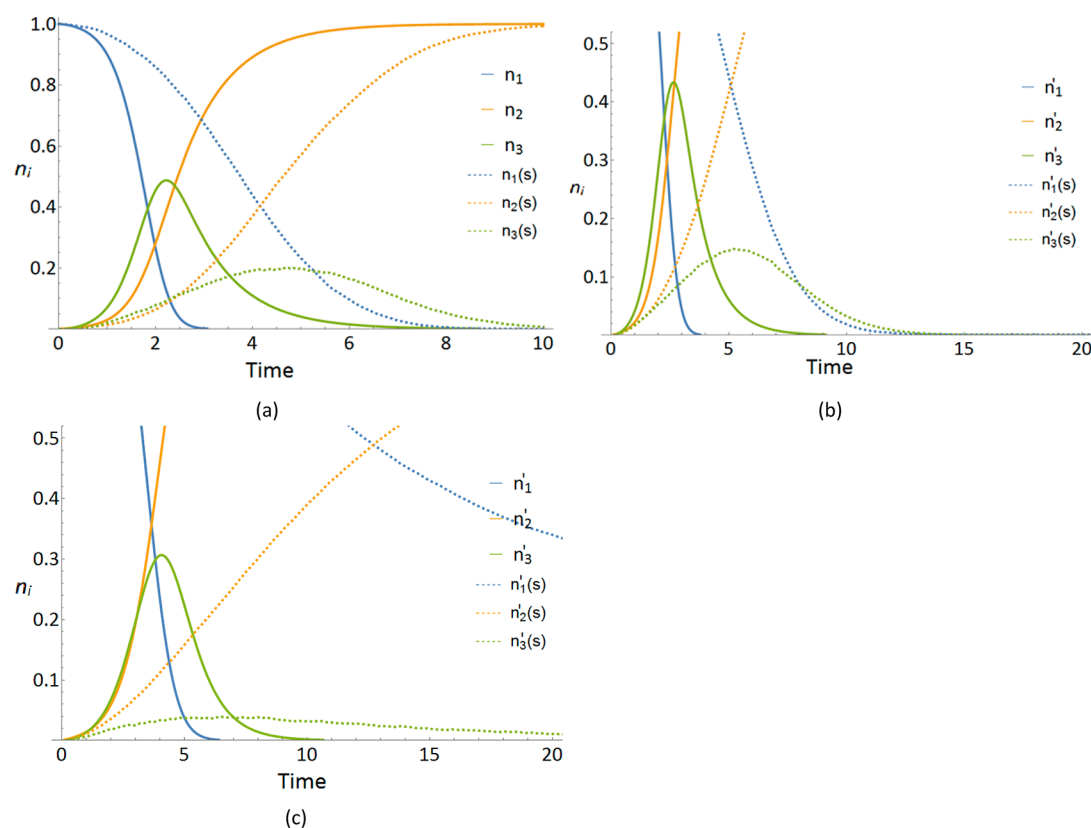
Figure 13. (a) Comparison of mean field (solid lines) and stochastic simulations (dotted lines) with no vacancies: $m = 6$; $k_{12} = 0.01$, $k_{13} = 10$; $k_{32} = 1$. (b, c) Comparison of normalized time-evolution curves for mean-field and stochastic simulations when vacancies in proton concentrations are present: (b) $n_4 = 0.3$, $k_{13}' = k_{13}(1 - n_4) = 7$; (c) $n = 0.7$, $k_{13}' = k_{13}(1 - n_4) = 3$. n_4 is the state probability that the proton site is a vacancy. The deactivation times increase by factors of 2 and 3, respectively, when $n_4 = 0.3$ and $n_4 = 0.7$.
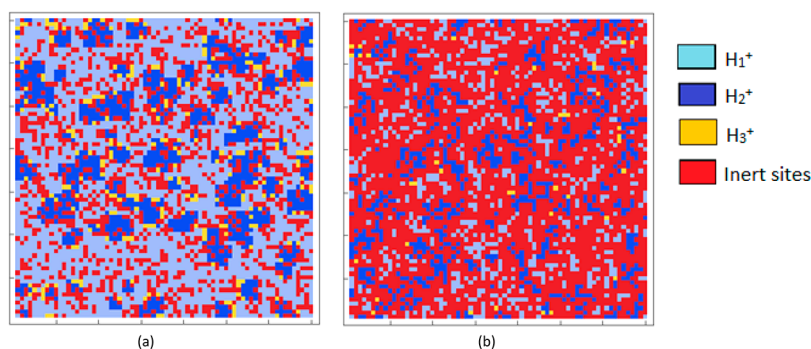
Figure 14. Distribution of proton state coverages in the stochastic simulations at different simulation times: (a) $n_4 = 0.3$ at time $t = 5$; (b) $n_4 = 0.7$ at time $t = 15$. Comparison of mode of propagation of deactivated proton state H_2^+ regions surrounded by proton state H_3^+ in a hexagonal lattice with $k_{12} = 0.01$, $k_{13} = 10$, and $k_{32} = 1$.

isolated. According to the stochastic simulations, H_1^+ sites already behave as if they are completely isolated when the vacancy concentration n_4 equals 0.5 (see Figure S13 and section SI 5.3 for more details).

Pattern formations of the respective proton states are responsible for this isolated site behavior. As Figure 14 illustrates, the distribution of proton state probability n_1 is no longer homogeneous around proton state probability n_2. Proton state H_3^+ regions grow around deactivated proton state H_2^+ regions. Since the deactivation rate of proton state H_1^+ is slower than that of proton state H_3^+, the system has to wait for the transient proton state H_3^+ layer that surrounds the deactivated proton state H_2^+ regions to decay. After decay, the proton state

H_3^+ generation process is restarted. Due to island formation, percolation of state probabilities H_2^+ has become reduced. This occurs when n_4 is 0.5, since this is near the percolation threshold[42] of a hexagonal lattice.

4.2. Stochastic Simulations of the Dual Interacting Proton Catalyst Model. Here we extend the analysis of section 4.1 with simulations for the dual interacting proton catalyst model as a function of surface vacancy concentration. The full kinetics according to the reaction cycle of Figure 8 is coupled to stochastic dynamics of the protons (for method details see section SI 5.4).

Stochastic simulations differ again from mean field simulations. However, remarkably, when the alkylation
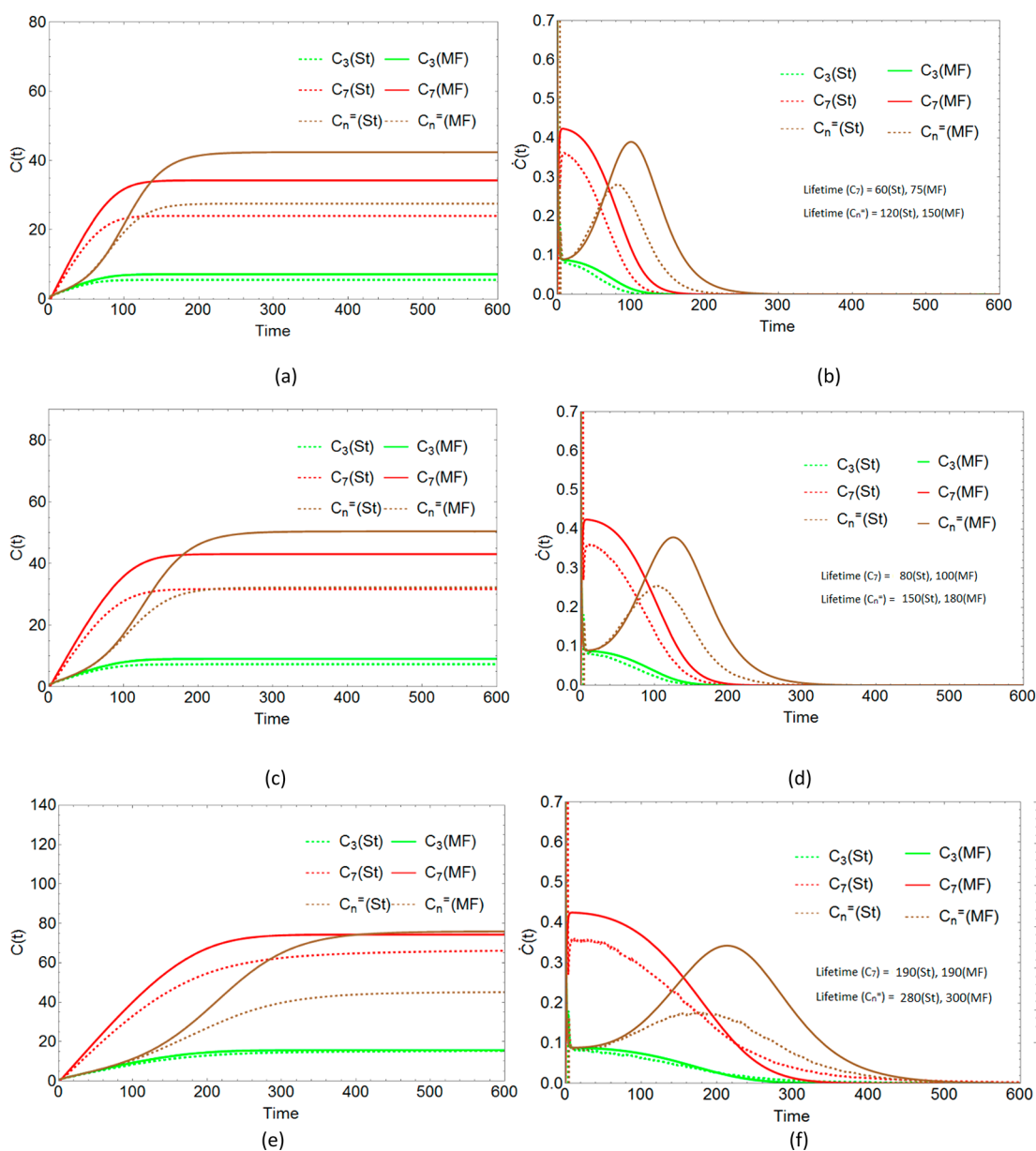
Figure 15. Mean field (solid lines) and stochastic simulations (dotted lines) of the dual interacting proton catalyst model for default parameters. Default kinetics parameters are the same as Figure 10, for a single proton case giving high alkylate production. (a, c, e) Product formation normalized and (b, d, f) rates of product formation with time and proton vacancy concentrations $n_4 = 0, 0.3, 0.7$, respectively. Product formation is plotted per initial density of H_1^+ sites. The rate of deactivation decreases subsequently as n_4 increases. For $n_4 = 0.7$, the alkylate deactivation rate is reduced in the stochastic simulations for longer times. For (b, d, f) the mean field steady state $S(C_7) = 63\%$ and stochastic steady state $S(C_7) = 60\%$.

selectivity is high (Figure 15), in contrast to the three proton state model stochastic simulations show now enhanced rates of deactivation and short catalyst lifetimes. Analogous to the three proton state model, delay of deactivation of oligomerization when alkylate production has deactivated becomes less.

When alkylation selectivity is low (Figure 17), one finds that the deactivation rate is decreased in comparison to the mean field simulation with longer catalyst lifetimes.

The differences between mean field and stochastic simulations relate to proton mobility limitations caused by surface overlayer patterns of adsorbed reaction intermediates.

In the figure legends, alkylation catalysis and oligomerization lifetimes are mentioned. Selectivities are mentioned in the respective captions to the figures.

The stochastic simulations of Figure 15a,b show a shorter catalyst lifetime of alkylate and oligomerization production in comparison to the mean field simulations. As was mentioned, this is due to pattern formation of reaction intermediates adsorbed on the surface lattice. Differently from the three proton state model, the surface becomes now also occupied by C_3^+, iC_4^+, and C_7^+ cations (see Figure 16a). Once a deactivated proton state H_2^+ is generated, it will have a reduced probability to meet a proton in state H_1^+. This will reduce the initial rate of proton state H_3^+ generation. Because proton state H_3^+ dominates the oligomer removal rate, oligomer production now is increased. This intermediate oligomer concentration then causes quicker deactivation of state H_1^+. A similar phenomenon happened in the dual noninteracting proton catalyst model, where the presence of slowly deactivating H_3^+
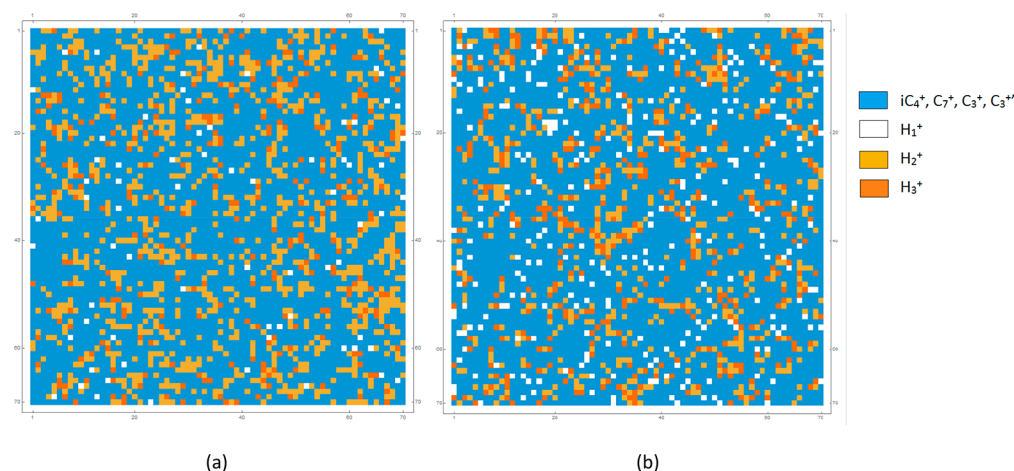
Figure 16. Plots of the site concentration on the lattice for (a) high alkylation selectivity and (b) low alkylation selectivity at times $t = 70$ and $t = 15$, respectively ($n_4 = 0$).
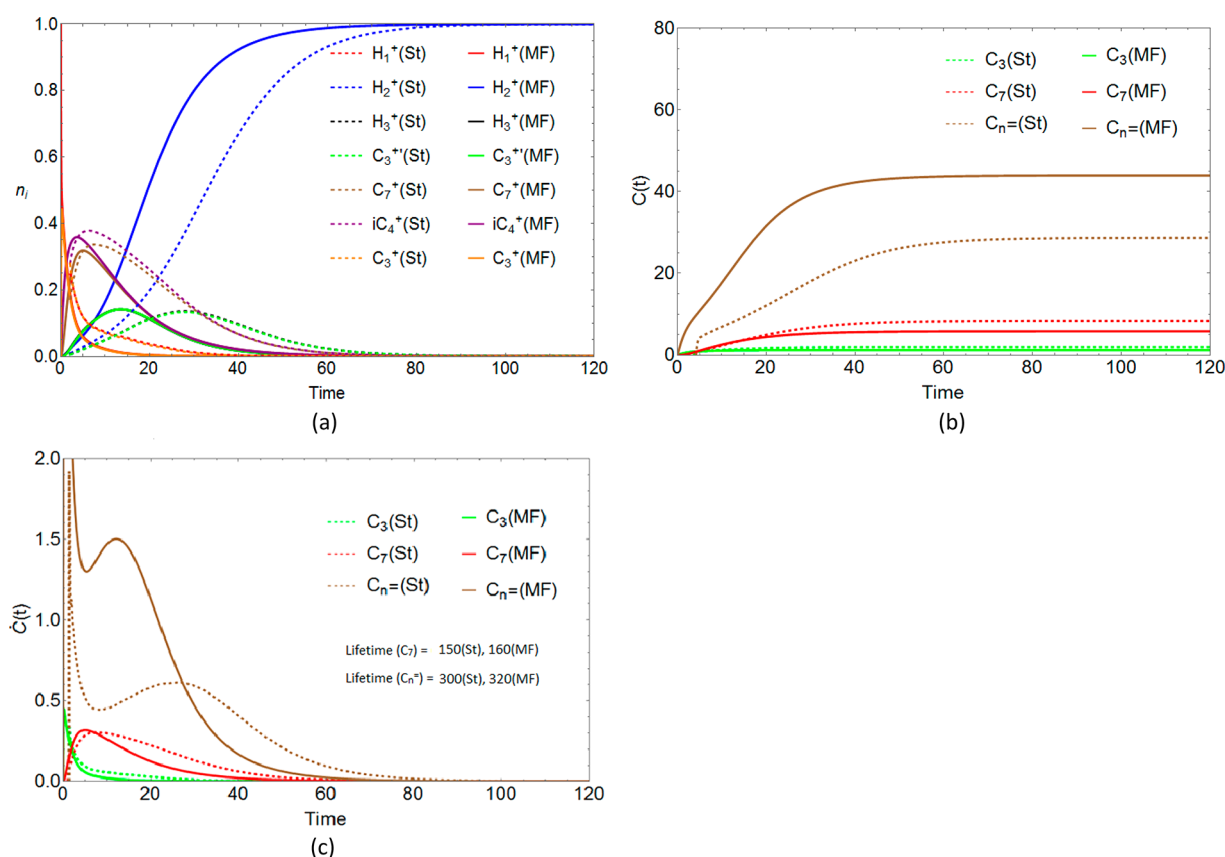
Figure 17. Single proton catalyst model: the case of low selectivity to alkylate formation. Comparison of mean field (solid line) and stochastic simulation (dotted lines) for the reaction network given in Figure 3. (a−c) Surface concentration, product formation, and rate of product formation as a function of time. $k_{10} = k_{10}' = 10$ ($k_1 = k_2 = k_4 = 1$, $k_3 = k_5 = 0.1$, $k_6 = k_7 = 0.01$, $k_8 = 10$, $k_9 = k_9' = 10$, $k_{11} = k_{11}' = 0.01$; steady state $S(C_7) = 19\%$ for mean field simulations and $S(C_7) = 31\%$ for stochastic simulations).

protons increased the deactivation rete of the H_1^+ protons (compare Figure 10d with Figure 10f).

With an increase in surface vacancies (Figure 15c−f), the mean field and stochastic simulations show an increasingly longer alkylation lifetime and slower deactivation time. In the stochastic simulations, the relative lifetime of alkylation increases more than in the mean field simulations, but the relative increase in lifetime of oligomerization is less, as is the case for the respective deactivation rates. The initial steady state

selectivity of alkylation does not change. When $n_4 = 0.7$, protons in stochastic simulations start to behave as isolated protons. This is due to the loss of H_2^+ percolation, as also discussed in section 4.1.1 (for more details, refer to section SI 6). Then in the mean-field simulation, the delay in peak oligomer formation is still 40 time steps.

Figure 17 shows that, when steady state alkylate selectivity is fast, oligomerization product formation always dominates. A double peak in oligomer production is observed. The first peak is

due to the H_1^+ protons that rapidly deactivate, and the latter maximum is from oligomer production by the proton in the H_3^+ state.

Different from what was observed in Figure 15, the stochastic simulations in Figure 17 now show a delay in the rate of deactivation of oligomer production by the H_3^+ proton states. The deactivation rate of proton state H_1^+ by $C_n^=$ is so rapid that the meeting probability with proton state H_2^+ dominates. A representative surface overlayer intermediate pattern is shown is Figure 16b. Because oligomer concentration is already high, a further change in oligomer concentration will have no significant effect. In the stochastic simulations, delayed formation of proton state H_3^+ is now the cause of the slower rate of decay.

5. CONCLUSION

In this paper, we have presented kinetic simulations of deactivation rates of the alkylation reaction of propylene with isobutane catalyzed by a variety of surface models of the solid acid catalyst. The question is addressed of how lateral interactions between protons will change catalyst stability and product distribution as a function of time.

Catalyst deactivation by protons that laterally interact has been computationally studied with a dual interacting proton catalyst model. In the dual interacting proton catalyst model initially only reactive protons are present that selectively produce alkylate. In time, they become deactivated. This induces still present reactive protons to convert to less reactive protons that now only catalyze propylene oligomerization. The latter reaction also deactivates in time.

The existence of protons selective to alkylation, different from protons that only oligomerize alkene oligomerization, is consistent with experiments[7,8,10,43−45] and theory.[26] Strongly acidic protons promote alkylate production over alkene oligomerization. This is because reactive protons favor the hydride transfer reaction between isobutane and carbenium ion versus the propylene oligomerization reaction. Catalyst deactivation occurs through two deactivation reaction channels that do not operate independently of each other.

Deprotonation of reaction intermediate carbenium ions will initiate catalyst deactivation by generation of alkenes. This leads to deactivation because of consecutive deactivating oligomerization reactions. This deactivation reaction channel is mainly operational at high alkylate selectivity.

This second deactivation reaction channel, which dominates when alkylate selectivity is low, is reactant alkene oligomerization. This reaction competes with the hydride transfer reaction that initiates the alkylation reaction.

The presence of these two deactivation channels is consistent with the two experimental selectivity regimes of high and low alkylate selectivity observed in the CSTR experiment.[10] Selective alkylation catalyzed by solid acid catalysts has to be done with high isobutane to alkene ratio under integral conditions in a CSTR that enables initially 100% conversion of reactant alkenes. This minimizes alkene concentration and provides a uniform distribution of reactant and product in the reactor. Then alkylate selectivity is high.[18] There is initially no observable catalyst deactivation. Catalyst deactivation becomes observable once catalyst protons have become deactivated such that the conversion of reactant alkene drops below 100%.

Experimentally the change in product selectivity as a function of reaction time can be followed also in the 100% propylene conversion regime. In this reaction regime where alkylation selectivity is high, a gradual decline in alkylate and alkane

production rate is observed.[10] In addition, a steady production rate increase of oligomer molecules happens that is derived from deprotonated carbenium ions. This shows that when alkylate selectivity is high the main deactivation is due to the deprotonation reactions of intermediate carbenium ions.

Because of ongoing deactivation in the experiment, conversion of alkene will at some point decrease to less than 100%. Due to the increased propylene reactant concentration, the rate of the propylene oligomerization reaction increases and the hydride transfer reaction rate will no longer be able to compete with it. Then, selective alkylate production decreases sharply and reactant alkene oligomers become the main product.[10]

These observations agree with kinetics simulations of the deactivation of the alkylation reaction. When alkylate selectivity is high, the main deactivation is due to disruption of the propagation reaction cycle through deprotonation of intermediate carbenium ions. When oligomer production dominates, the deprotonation reaction becomes replaced by deactivating alkene oligomerization as the main cause of catalyst deactivation.

Kinetics simulations with the dual interacting proton catalyst model show that lateral interactions strongly and negatively affect the lifetime of the alkylation catalyst. Additionally, it is found that, due to the increased rate of alkylate deactivation, oligomer production continues after deactivation of alkylate production.

Whereas, as a function of time, the CSTR experiment shows initially high alkylation activity and delayed oligomer production when alkylate selectivity declines, this is no indication that lateral interactions as discussed in this paper play a role. In the experiment that initially converts alkene 100%, the decline of alkylate production followed by an increase of oligomer production is the result of the sudden increase in alkene concentration. This happens when alkene conversion decreases to less than 100% due to gradual loss of reactive protons.

In the simulations, we have compared kinetics of the dual interacting proton catalyst model with two other catalyst models: a single proton catalyst model and a dual catalyst noninteracting proton catalyst model. In the absence of lateral interactions, it is found that an increased local proton concentration will also increase catalyst deactivation rate. It increases locally the concentration of alkene intermediates that rapidly deactivate the catalyst. Therefore, a reduced surface concentration of protons is beneficial to catalyst lifetime. Experiments by Mores et al.[5] on the deactivation of the MTO reaction report a related proton concentration effect that extends catalyst lifetime. In reference to a study by Schüßler et al.,[45] which deals with the alkylation reaction, it is also reported that a decreased proton concentration enhances the lifetime of the catalyst.

A comparison of the dual interacting proton catalyst model and a dual catalyst noninteracting catalyst model shows that, even in the absence of lateral interactions, the additional presence of protons that only catalyze propylene oligomerization has a large negative effect on catalyst selectivity and also reduces catalyst life. When alkylation is ongoing, oligomer production by protons that are not selective to alkylate production is much faster than that by the alkylate-producing protons. Experimental results[10] confirm the conclusion that the additional presence of weakly reactive sites decreases catalyst life.

Nonlinear dynamics analysis suggests that the deactivation kinetics of laterally interacting protons as simulated with the

dual interacting proton catalyst model is not necessarily specific to the alkylation reaction. It may occur in reactions catalyzed by laterally interacting protons that require highly reactive protons for selective production of a desirable product. Examples of such reactions in addition to the alkylation reaction are the MTO reaction or the catalytic cracking reaction.[46] Interestingly, this implies that the effect is expected to be absent in hydrocracking or hydroisomerisation reactions, which are less sensitive to proton reactivity since conversions of intermediate olefins are then reaction rate controlling.[20]

Stochastic simulations have been compared with mean field simulations. Stochastic simulations find differences with mean field simulations since adsorbed reaction intermediates are not homogeneously distributed on the working catalyst. When these simulations are applied to the dual interacting proton catalyst model, one finds that coverage of the surface by reaction intermediates inhibits additional conversion of reactive protons into weakly reactive protons. Because of the large difference in overall oligomer production rates between reactive protons, which catalyze alkylation, and weakly reactive protons, which only catalyze oligomerization, this affects a selective alkylation catalyst differently from a catalyst that dominantly produces oligomers. In comparison to mean field simulations, it reduces the lifetime of a selective alkylation catalyst but makes it slightly longer when alkylation selectivity is low. The stochastic simulations show that laterally interacting protons behave kinetically as isolated protons, when on a hexagonal lattice the proton vacancy concentration is in excess of 50%.

■ ASSOCIATED CONTENT

Ⓢ Supporting Information

The Supporting Information is available free of charge on the ACS Publications website at DOI: 10.1021/acscatal.8b01511.

> Mean-field solutions of kinetic equations for single reactivity and dual interacting and dual noninteracting proton catalyst models, three proton state model with mean-field analysis with phase portraits and comparison with stochastic simulations, and stochastic simulations of the dual interacting proton catalyst model (PDF)

■ AUTHOR INFORMATION

Corresponding Author

*E-mail for R.A.v.S.: r.a.v.santen@tue.nl.

ORCID Ⓞ

Rutger A. van Santen: 0000-0003-1835-4520

Johan Padding: 0000-0003-4161-0748

Notes

The authors declare no competing financial interest.

■ ACKNOWLEDGMENTS

■ REFERENCES

(1) Ertl, G. *Reactions at Solid Surfaces*; Wiley: Hoboken, NJ, USA, 2009.

(2) Derouane, E. G.; Védrine, J. C.; Pinto, R. R.; Borges, P. M.; Costa, L.; Lemos, M. A. N. D. A.; Lemos, F.; Ribeiro, F. R. The Acidity of Zeolites: Concepts, Measurements and Relation to Catalysis: A Review on Experimental and Theoretical Methods for the Study of Zeolite Acidity. *Catal. Rev.: Sci. Eng.* **2013**, *55*, 454–515.

(3) van Santen, R. A.; Kramer, G. J. Reactivity Theory of Zeolitic Broensted Acidic Sites. *Chem. Rev.* **1995**, *95*, 637–660.

(4) Di Iorio, J. R.; Nimlos, C. T.; Gounder, R. Introducing Catalytic Diversity into Single-Site Chabazite Zeolites of Fixed Composition via Synthetic Control of Active Site Proximity. *ACS Catal.* **2017**, *7*, 6663–6674.

(5) Mores, D.; Kornatowski, J.; Olsbye, U.; Weckhuysen, B. M. Coke Formation during the Methanol-to-Olefin Conversion: In Situ Microspectroscopy on Individual H-ZSM-5 Crystals with Different Brønsted Acidity. *Chem. - Eur. J.* **2011**, *17*, 2874–2884.

(6) Bartholomew, C. H.; Farrauto, R. J. Catalyst Deactivation: Causes, Mechanisms, and Treatment. In *Fundamentals of Industrial Catalytic Processes*; Wiley: Hoboken, NJ, USA, 2010; pp 260–336.

(7) Corma, A.; Martínez, A. Chemistry, Catalysts, and Processes for Isoparaffin−Olefin Alkylation: Actual Situation and Future Trends. *Catal. Rev.: Sci. Eng.* **1993**, *35*, 483–570.

(8) Feller, A.; Lercher, J. A. Chemistry and Technology of Isobutane/Alkene Alkylation Catalyzed by Liquid and Solid Acids. *Adv. Catal.* **2004**, *48*, 229–295.

(9) Weitkamp, J.; Traa, Y. Isobutane/butene Alkylation on Solid Catalysts. Where Do We Stand? *Catal. Today* **1999**, *49*, 193–199.

(10) Feller, A.; Guzman, A.; Zuazo, I.; Lercher, J. A. On the Mechanism of Catalyzed Isobutane/butene Alkylation by Zeolites. *J. Catal.* **2004**, *224*, 80–93.

(11) Feller, A.; Barth, J.-O.; Guzman, A.; Zuazo, I.; Lercher, J. A. Deactivation Pathways in Zeolite-Catalyzed Isobutane/butene Alkylation. *J. Catal.* **2003**, *220*, 192–206.

(12) D'Amico, V.; Gieseman, J.; Nousiainen, H.; van Broekhoven, E.; van Rooijen, E. Consider New Methods to Debottleneck Clean Alkylate Production. *Hydrocarb. Process.* **2006**, 65–70.

(13) Broekhoven, E. H.; van Rooijen, E. Alkylation with Solid Acid Catalyst. *Pet. Technol. Q.* **2008**, *13*, 87–93.

(14) Olsbye, U.; Svelle, S.; Lillerud, K. P.; Wei, Z. H.; Chen, Y. Y.; Li, J. F.; Wang, J. G.; Fan, W. B. The Formation and Degradation of Active Species during Methanol Conversion over Protonated Zeotype Catalysts. *Chem. Soc. Rev.* **2015**, *44*, 7155–7176.

(15) Brillis, A. A.; Manos, G. Catalyst Deactivation during Catalytic Cracking of N-Octane, Isooctane and 1-Octene over USHY Zeolite at Mild Conditions and Short Times on Stream. *Stud. Surf. Sci. Catal.* **2001**, *139*, 255–262.

(16) Wojciechowski, B. W.; Corma, A. *Catalytic Cracking: Catalysts, Chemistry, and Kinetics*, 1st ed.; M. Dekker: New York, 1986.

(17) Janssens, T. V. W.; Svelle, S.; Olsbye, U. Kinetic Modeling of Deactivation Profiles in the Methanol-to-Hydrocarbons (MTH) Reaction: A Combined Autocatalytic−hydrocarbon Pool Approach. *J. Catal.* **2013**, *308*, 122–130.

(18) De Jong, K. P.; Mesters, C. M. A. M.; Peferoen, D. G. R.; Van Brugge, P. T. M.; De Groot, C. Paraffin Alkylation Using Zeolite Catalysts in a Slurry Reactor: Chemical Engineering Principles to Extend Catalyst Lifetime. *Chem. Eng. Sci.* **1996**, *51*, 2053–2060.

(19) van Santen, R. A.; Liu, C. Theory of Zeolite Catalysis. In *Modelling and Simulation in the Science of Micro- and Meso-Porous Materials*; Elsevier: Amsterdam, 2018; pp 151–188.

(20) van Santen, R. A. Solid Acid Catalysis, Theory and Reaction Mechanisms. In *Modern heterogeneous catalysis: an Introduction*; Wiley-VCH: Weinheim, Germany, 2017; p 592.

(21) Haw, J. F.; Song, W.; Marcus, D. M.; Nicholas, J. B. The Mechanism of Methanol to Hydrocarbon Catalysis. *Acc. Chem. Res.* **2003**, *36*, 317–326.

(22) Olsbye, U.; Svelle, S.; Bjørgen, M.; Beato, P.; Janssens, T. V. W.; Joensen, F.; Bordiga, S.; Lillerud, K. P. Conversion of Methanol to Hydrocarbons: How Zeolite Cavity and Pore Size Controls Product Selectivity. *Angew. Chem., Int. Ed.* **2012**, *51*, 5810–5831.

(23) Weitkamp, J. Catalytic Hydrocracking-Mechanisms and Versatility of the Process. *ChemCatChem* **2012**, *4*, 292–306.

(24) Bibby, D. M.; Howe, R. F.; Mclellan, G. D. Coke Formation in High-Silica Zeolites. *Appl. Catal., A* **1992**, *93*, 1–34.

(25) Schmerling, L. The Mechanism of the Alkylation of Paraffins. *J. Am. Chem. Soc.* **1945**, *67*, 1778–1783.

(26) Liu, C.; van Santen, R. A.; Poursaeidesfahani, A.; Vlugt, T. J. H.; Pidko, E. A.; Hensen, E. J. M. Hydride Transfer versus Deprotonation Kinetics in the Isobutane−Propene Alkylation Reaction: A Computational Study. *ACS Catal.* **2017**, *7*, 8613−8627.

(27) Tuma, C.; Kerber, T.; Sauer, J. The Tert-Butyl Cation in H-Zeolites: Deprotonation to Isobutene and Conversion into Surface Alkoxides. *Angew. Chem., Int. Ed.* **2010**, *49*, 4678−4680.

(28) Rozanska, X.; van Santen, R. A.; Demuth, T.; Hutschka, F.; Hafner, J. A Periodic DFT Study of Isobutene Chemisorption in Proton-Exchanged Zeolites: Dependence of Reactivity on the Zeolite Framework Structure. *J. Phys. Chem. B* **2003**, *107*, 1309−1315.

(29) Janik, M. J.; Davis, R. J.; Neurock, M. A Density Functional Theory Study of the Alkylation of Isobutane with Butene over Phosphotungstic Acid. *J. Catal.* **2006**, *244*, 65−77.

(30) Kazansky, V. B.; Frash, M. V.; van Santen, R. A. A Quantum-Chemical Study of Hydride Transfer in Catalytic Transformations of Paraffins on Zeolites. Pathways through Adsorbed Nonclassical Carbonium Ions. *Catal. Lett.* **1997**, *48*, 61−67.

(31) Liu, C.; Tranca, I.; van Santen, R. A.; Hensen, E. J. M.; Pidko, E. A. Scaling Relations for Acidity and Reactivity of Zeolites. *J. Phys. Chem. C* **2017**, *121*, 23520−23530.

(32) Sievers, C.; Liebert, J. S.; Stratmann, M. M.; Olindo, R.; Lercher, J. A. Comparison of Zeolites LaX and LaY as Catalysts for isobutane/2-Butene Alkylation. *Appl. Catal., A* **2008**, *336*, 89−100.

(33) Schüßler, F.; Pidko, E. A.; Kolvenbach, R.; Sievers, C.; Hensen, E. J. M.; van Santen, R. A.; Lercher, J. A. Nature and Location of Cationic Lanthanum Species in High Alumina Containing Faujasite Type Zeolites. *J. Phys. Chem. C* **2011**, *115*, 21763−21776.

(34) Van Santen, R. A.; Sengar, A.; Steur, E. The Challenge of Catalyst Prediction. *Faraday Discuss.* **2018**.

(35) Marin, G. B.; Yablonsky, G. S. *Kinetics of Chemical Reactions*; Wiley-VCH: Weinheim, Germany, 2011.

(36) Feller, A.; Zuazo, I.; Guzman, A.; Barth, J. O.; Lercher, J. A. Common Mechanistic Aspects of Liquid and Solid Acid Catalyzed Alkylation of Isobutane with N-Butene. *J. Catal.* **2003**, *216*, 313−323.

(37) Sarazen, M. L.; Doskocil, E.; Iglesia, E. Catalysis on Solid Acids: Mechanism and Catalyst Descriptors in Oligomerization Reactions of Light Alkenes. *J. Catal.* **2016**, *344*, 553−569.

(38) Strogatz, S. H. *Nonlinear Dynamics and Chaos: With Applications to Physics, Biology, Chemistry, and Engineering*, 2nd ed.; Westview Press: Boulder, CO, USA, 2015.

(39) Dean, P.; Bird, N. F. Monte Carlo Estimates of Critical Percolation Probabilities. *Math. Proc. Cambridge Philos. Soc.* **1967**, *63*, 477.

(40) Jacobsen, J. L. High-Precision Percolation Thresholds and Potts-Model Critical Manifolds from Graph Polynomials. *J. Phys. A: Math. Theor.* **2014**, *47*, 135001.

(41) Suding, P. N.; Ziff, R. M. Site Percolation Thresholds for Archimedean Lattices. *Phys. Rev. E: Stat. Phys., Plasmas, Fluids, Relat. Interdiscip. Top.* **1999**, *60*, 275−283.

(42) Sykes, M. F.; Essam, J. W. Exact Critical Percolation Probabilities for Site and Bond Problems in Two Dimensions. *J. Math. Phys.* **1964**, *5*, 1117−1127.

(43) Mostad, H. B.; Stöcker, M.; Karlsson, A.; Rørvik, T. Comparison of the iso-structural H-SAPO-37 and H-faujasite as catalysts for the isobutane/2-butene alkylation. *Appl. Catal., A* **1996**, *144*, 305−317.

(44) Corma, A.; Martínez, A.; Martínez, C. Isobutane/2-butene alkylation on ultrastable Y zeolites: Influence of zeolite unit cell size. *J. Catal.* **1994**, *146*, 185−192.

(45) Schüßler, F.; Schallmoser, S.; Shi, H.; Haller, G. L.; Ember, E.; Lercher, J. A. Enhancement of Dehydrogenation and Hydride Transfer by La^{+3} Cations in Zeolites during Acid Catalyzed Alkane Reactions. *ACS Catal.* **2014**, *4*, 1743−1752.

(46) Corma, A.; Orchillés, A. V. Current views on the mechanism of catalytic cracking. *Microporous Mesoporous Mater.* **2000**, *35−36*, 21−30.